AGU PUBLICATIONS

Global Biogeochemical Cycles

RESEARCH ARTICLE
10.1002/2017GB005792

Key Points:
- Nitrous oxide measurements are used to correct for mixing fluxes in ship-based estimates of net community production
- The magnitude of the mixing correction is highest in coastal waters during spring and summer upwelling
- Corrected net community production shows better coherence with hydrographic variables than uncorrected values

Supporting Information:
- Supporting Information S1

Correspondence to:
R. W. Izett,
rizett@eoas.ubc.ca

Citation:
Izett, R. W., Manning, C. C., Hamme, R. C., & Tortell, P. D. (2018). Refined estimates of net community production in the Subarctic Northeast Pacific derived from ΔO_2/Ar measurements with N_2O-based corrections for vertical mixing. *Global Biogeochemical Cycles*, *32*. https://doi.org/10.1002/2017GB005792

Received 29 AUG 2017
Accepted 7 FEB 2018
Accepted article online 12 FEB 2018

Refined Estimates of Net Community Production in the Subarctic Northeast Pacific Derived From ΔO_2/Ar Measurements With N_2O-Based Corrections for Vertical Mixing

Robert W. Izett[1], Cara C. Manning[1], Roberta C. Hamme[2], and Philippe D. Tortell[1,3,4]

[1]Department of Earth, Ocean and Atmospheric Sciences, University of British Columbia, Vancouver, British Columbia, Canada, [2]School of Earth and Ocean Sciences, University of Victoria, Victoria, British Columbia, Canada, [3]Botany Department, University of British Columbia, Vancouver, British Columbia, Canada, [4]Peter Wall Institute for Advanced Studies, University of British Columbia, Vancouver, British Columbia, Canada

Abstract We present the first field application of a N_2O-based approach to correct for vertical mixing in the estimation of net community production (NCP) from mixed layer O_2 measurements. Using new ship-based observations of N_2O and biological oxygen saturation anomalies (ΔO_2/Ar) from the Subarctic Northeast Pacific, we provide refined mixed layer NCP estimates across contrasting hydrographic regimes and a comprehensive assessment of the methodological considerations and limitations of the approach. Increased vertical mixing coefficients at the base of the mixed layer, derived using N_2O measurements, corresponded with periods of heightened wind speed and coastal upwelling. Corrections were most significant in coastal regions where the vertical supply of low-O_2 water can otherwise falsely imply net heterotrophy from negative ΔO_2/Ar measurements. After correcting for the mixing flux, all coastal stations showed autotrophic signatures, with maximum NCP exceeding 100 mmol O_2 m^{-2} d^{-1} in the spring and summer. Vertical fluxes were lower in off-shelf waters but often contributed more than 50% to corrected NCP. At some oceanic stations, however, the cooccurrence of N_2O minima and O_2 maxima resulted in biased (overestimated) N_2O corrections. Evaluating vertical fluxes in these regions remains a challenge for ship-based studies. Nonetheless, our refined NCP estimates show better coherence with surface chlorophyll, temperature, and mixed layer depth than uncorrected values. Potential mixed layer N_2O production introduces some uncertainty in the approach, but errors are likely to be small. Ultimately, this work provides rationale for the adoption of the N_2O correction to refine NCP estimates, particularly in coastal waters.

1. Introduction

Marine organic carbon production via photosynthesis regulates higher trophic level biomass (Ware & Thomson, 2005) and influences the strength of the ocean's biological pump (Volk & Hoffert, 1985). Accurate quantification of primary production is thus critical for understanding the functioning of marine ecosystems and their response to environmental change. As a currency of life, oxygen (O_2) can be used as a tracer of biological production in the ocean. The net community production (NCP) of O_2 represents the balance between primary production and community respiration (both autotrophic and heterotrophic) and is equivalent to carbon export at steady state and on interannual timescales (Laws, 1991).

A number of field studies have previously quantified NCP by examining the mixed layer O_2 mass balance (e.g., Emerson et al., 1997; Giesbrecht et al., 2012; Luz & Barkan, 2009; Reuer et al., 2007). One common approach is to normalize O_2 concentrations to argon (Ar), a biologically inert gas, with solubility and diffusivity properties that are nearly identical to O_2 (Craig & Hayward, 1987). This normalization removes the influence of physical processes, such as bubble injection and temperature change, that affect O_2 saturation state. Following Kaiser et al. (2005) and Reuer et al. (2007), steady state NCP (mmol O_2 m^{-2} d^{-1}) is equated to the air-sea flux of biologically produced O_2:

$$\mathrm{NCP} = \Delta O_2/\mathrm{Ar}\cdot[O_2]_{eq}\cdot k_{O_2}, \quad (1)$$

where ΔO_2/Ar is the biological O_2 saturation anomaly (unitless; equation (2)), $[O_2]_{eq}$ is the O_2 equilibrium concentration (mmol m^{-3}), and k_{O_2} is the gas transfer velocity of O_2 (m d^{-1}).

Developments in sea-going mass spectrometry over the past decade (Cassar et al., 2009; Kaiser et al., 2005; Tortell, 2005) have made it possible to obtain high-resolution estimates of NCP using continuous ship-board measurements of O_2/Ar. High spatial sampling resolution is achieved, and biases associated with discrete methods for measuring primary production are avoided, making this approach ideal for open-ocean environments. A number of groups have now applied ship-based ΔO_2/Ar measurements in a variety of regions, greatly expanding the spatial coverage of NCP data (Hamme et al., 2012; Kaiser et al., 2005; Lockwood et al., 2012; Manning et al., 2017; Stanley et al., 2010; Tortell et al., 2015, 2012; Ulfsbo et al., 2014).

Despite significant advances in NCP measurements, current estimates remain limited by uncertainty in the contribution of vertical mixing to the surface O_2 budget (Hamme & Emerson, 2006). When O_2 is undersaturated (supersaturated) beneath the mixed layer, failure to account for the mixing supply of this low-O_2 (high-O_2) water (through mixed layer entrainment or vertical diffusivity and advection) can lead to an underestimation (overestimation) of derived NCP. This problem has been widely recognized, particularly in coastal regions, and limits the applicability of ΔO_2/Ar as a productivity tracer (Giesbrecht et al., 2012; Hamme & Emerson, 2006; Jonsson et al., 2013). In some cases, such regions may falsely appear to be net heterotrophic unless a mixing correction is made.

Recent modeling work by Cassar et al. (2014) has suggested that measurements of nitrous oxide (N_2O), within and below the mixed layer, may be used to trace vertical mixing and correct ΔO_2/Ar-based NCP estimates. Nitrous oxide is largely produced in the oceans during organic matter remineralization, as a by-product of ammonium oxidation (AO) to nitrate (i.e., nitrification) (Ward, 2000). As a result, a consistent relationship between the N_2O surplus and O_2 deficit is observed in much of the world's subsurface oceans (Cohen & Gordon, 1979; Nevison et al., 2003; Yoshinari, 1976). Vertical mixing, including advection, diffusion, and entrainment, can therefore provide a source of water that is both undersaturated in O_2 and supersaturated in N_2O. Such a signature has been observed in surface waters of upwelling margins globally (Bange et al., 1996; Capelle & Tortell, 2016). It has generally been believed that nitrification is photoinhibited and primarily constrained to subsurface waters (Horrigan et al., 1981). Mixed layer N_2O supersaturation is thus assumed to largely reflect vertical mixing, such that surface N_2O measurements can, in theory, be used to track the upward transport of low-O_2 water. To our knowledge, there have not yet been any direct tests of this method and its assumptions with field data.

In this article, we present new NCP estimates from the Subarctic NE Pacific Ocean, using N_2O-corrected ship-based measurements of ΔO_2/Ar across a range of coastal (on-shelf) and open-ocean (off-shelf) waters. Surface productivity in the off-shelf waters of the Subarctic Pacific is limited by iron (Fe) availability during the summer (Boyd et al., 1996; Maldonado et al., 1999), while the persistence of a steep halocline and strong density stratification (Tabata, 1975) limits exchange between the surface and subsurface. In contrast, coastal waters of this region are characterized by complex physical dynamics, including seasonal upwelling and mixing over heterogeneous bottom topography (Crawford & Thomson, 1991; Whitney et al., 2005). These physical processes drive high productivity but also introduce uncertainty in ΔO_2/Ar-based NCP estimates. Our study thus presents an opportunity to evaluate O_2-based estimates of NCP across contrasting oceanographic regimes. Our new observations provide refined estimates of NCP in the Subarctic Pacific and demonstrate that neglecting the physical contributions to the mixed layer O_2 budget can lead to significant underestimates in some cases. We also evaluate the seasonal and spatial trends in NCP and present an in-depth evaluation of the limitations, uncertainties, and methodological considerations of the N_2O correction approach. Our work builds on that of Cassar et al. (2014) and provides guidance for future studies.

2. Methods

2.1. Study Area

We collected data on five oceanographic cruises in the Subarctic NE Pacific on the *CCGS John P. Tully*, between February and September 2016 (Figure 1). Line P cruises to Ocean Station Papa (OSP/Station P26; 50°N, 145°W) were conducted in winter (February), spring (June), and summer (August), covering a transect from the coastal Juan de Fuca (JF) Strait and southern West Coast Vancouver Island (WCVI) to the open-ocean waters of the Gulf of Alaska. Coastal waters around Vancouver Island, including the JF and WCVI regions, were

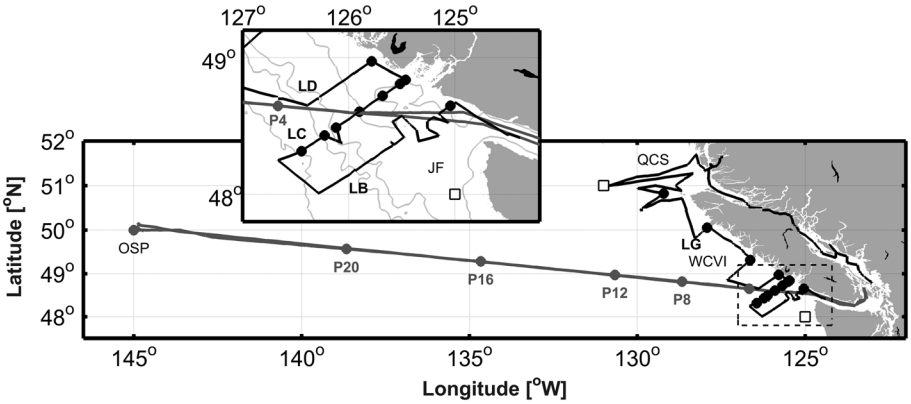

Figure 1. Map of representative Line P (gray) and La Perouse (black) cruise tracks, with markers showing the locations of N_2O profile sampling. The contour lines on the inset represent the 100, 500, 1,000, and 2,000 m isobaths. JF, WCVI, and QCS denote the Juan de Fuca canyon, West Coast Vancouver Island, and Queen Charlotte Sound regions, respectively. P4, P8, P12, P16, P20, and OSP (P26) represent the major Line P stations, and LB, LC, LD, and LG refer to transects along the La Perouse sampling grid. Note that the ship tracks varied slightly between cruises and that discrete surface samples for N_2O measurements were collected at higher spatial resolution than the plot markers (not shown). The inset shows an expanded view of the JF and southern WCVI regions. The open squares indicate the locations at which Bakun Upwelling Index values were obtained (Figure S5).

surveyed extensively during cruises in May and September, as part of the La Perouse monitoring program, run by Fisheries and Oceans Canada.

The WCVI region is generally influenced by the seasonal timing and intensity of summer upwelling and winter downwelling (Bylhouwer et al., 2013). During the summer and fall, local currents near the mouth of the JF region enhance upward transport of low-O_2, nutrient-rich deep water onto the shelf (Crawford & Peña, 2013). In the open-ocean waters of our survey region, strong winter winds drive upper ocean turbulence and mixed layer deepening, whereas increased solar radiation and weaker winds in the summer cause shoaling (Whitney & Freeland, 1999). In the spring, water column stratification enhances phytoplankton growth and nutrient drawdown prior to the onset of off-shelf summer macronutrient and Fe limitation and subsequent resupply via turbulent winter mixing (Peña & Varela, 2007; Whitney & Freeland, 1999). Year-round, deep mixing in the off-shelf waters is restricted by the presence of a steep halocline.

2.2. Underway O_2/Ar Measurements

Continuous measurements of mixed layer O_2/Ar were conducted using membrane inlet mass spectrometry (Tortell et al., 2011), with a *Hiden Analytical HAL20* quadrupole mass spectrometer. Seawater from the ship's underway seawater loop (intake at 4.5 m) was circulated at constant flow rate through rigid polypropylene tubing, past a 0.007″ thick water-impermeable silicone membrane. To minimize changes in the membrane gas permeability, which can affect measurements of O_2 and Ar, we maintained constant temperature (10°C) of inflowing seawater by circulating the water through a 6 m heat exchange coil immersed in a water bath. Measurements were obtained every ~20 s as the ratio of ion currents at the mass-to-charge ratios of 32 and 40 and averaged into 1 min bins.

Seawater standards, used to correct for instrument drift and to derive biological O_2 saturation anomalies (see section 2.4), consisted of air-equilibrated, 0.2 μm filtered seawater in 4 L polycarbonate bottles (Tortell et al., 2011). The bottles were incubated at ambient sea surface temperature (SST) and bubbled using an air pump to obtain gas equilibration with the atmosphere. While bubbling can introduce supersaturation in O_2, it negligibly affects the O_2/Ar ratio. At 2 h intervals, we measured the standards for 2 min, using the same flow rate and sampling temperature as during the underway data acquisition.

2.3. N_2O Sample Collection

Discrete samples for N_2O analysis were collected on all cruises from Niskin bottles. Depth profiles were obtained at various stations along the respective cruise tracks (markers in Figure 1), while surface measurements (5 m Niskin bottles) of N_2O supersaturation were collected at higher spatial resolution. During the August Line P trip, additional samples for surface N_2O analysis were obtained in the main laboratory

directly from the ship's underway seawater system. These samples and corresponding Niskin samples (obtained at the same station from 5 m Niskin bottles) showed good agreement (average root-mean-square error of 0.5 μmol m^{-3}; Figure S1 in the supporting information), and no statistically significant difference was observed between paired samples (n = 12). Underway samples obtained between stations were therefore included in our data.

For all N_2O measurements, duplicate subsamples were collected into 60 mL glass vials using flexible silicone tubing. The vials were overfilled three volumes avoiding bubble contamination, immediately poisoned with 50 μL saturated mercuric chloride ($HgCl_2$), and stored at 4°C in the dark until analysis (within 3 months). Nitrous oxide was measured in the laboratory using an automated purge-and-trap gas chromatography, mass spectrometry system (Capelle et al., 2015). Measurement precision was 3.5%, based on the average percent standard deviation of 125 triplicate air-equilibrated standards processed at the same time as our seawater samples.

2.4. Calculations of NCP

Uncorrected mixed layer NCP was calculated according to equation (1), where the biological O_2 saturation anomaly is defined, as per Craig and Hayward (1987), as

$$\Delta O_2/Ar = \frac{[O_2/Ar]_{meas}}{[O_2/Ar]_{eq}} - 1. \quad (2)$$

The *meas* and *eq* subscripts refer to the seawater and atmospheric equilibrium ratios measured from the underway seawater system and the bubbled air standards, respectively.

We calculated corrected NCP (mmol O_2 m^{-2} d^{-1}) following the approach of Cassar et al. (2014), which combines the mixed layer O_2 and N_2O budgets.

$$NCP = k_{O_2} \cdot \left(\Delta O_2/Ar \cdot [O_2]_{eq} - \frac{k_{N_2O}}{k_{O_2}} \cdot \frac{\partial [O_2]^B}{\partial [N_2O]^B} \cdot [N_2O]^B \right) \quad (3)$$

Here k_{N_2O} is the gas transfer velocity for N_2O (m d^{-1}), $\frac{\partial [O_2]^B}{\partial [N_2O]^B}$ is the vertical gradient of biological-O_2 to biological-N_2O concentrations (mmol O_2 (mmol N_2O)$^{-1}$), and $[N_2O]^B$ is the surface biological-N_2O saturation concentration (mmol N_2O m^{-3}). Cassar et al. (2014) assumed a constant $\frac{k_{N_2O}}{k_{O_2}}$ ratio of 0.92, but we independently calculated the ratio (range 0.87–0.94) for each observation based on the Schmidt number parameterizations reported in Wanninkhof (2014). The approach assumes that N_2O production (through nitrification) is photoinhibited in the mixed layer, but we discuss this assumption below (section 4.1.2). The NCP correction terms (i.e., the second part of equation (3)), obtained at each station with surface N_2O measurements (mean spatial resolution of approximately 102, 37, and 47 km in winter, spring, and summer respectively), were linearly interpolated to the resolution of the underway $\Delta O_2/Ar$ data (mean spatial resolution of 0.2 km). The interpolated correction terms were thus applied to equation (1) to obtain high-resolution estimates of NCP along our entire cruise tracks. We assume steady state in biological O_2 concentrations, and that horizontal fluxes of O_2 can be neglected in calculating NCP (see sections 4.1.5.3 and S2 of the supporting information for an analysis of these assumptions).

As measurements of O_2/Ar reflect processes occurring over the residence time of O_2 within the mixed layer (between approximately 1 and 4 weeks), we applied the approach of Reuer et al. (2007), with corrections by Teeter (2014), to calculate weighted gas transfer velocities for O_2 and N_2O over a 30 day period prior to our observations. We used the gas transfer velocity parameterization of Ho et al. (2006) based on 6-hourly CCMP (Cross-Calibrated Multi-Platform) wind vector analysis product data (retrieved from http://www.remss.com/measurements/ccmp/; Atlas et al., 2011).

The $[O_2]^B$ and $[N_2O]^B$ concentrations (mmol m^{-3}) represent the biological saturation concentrations of the respective gases. Within the mixed layer, $[O_2]^B$ is defined as

$$[O_2]^B = \Delta O_2/Ar \cdot [O_2]_{eq}, \quad (4)$$

where $\Delta O_2/Ar$ (equation (2)) accounts for bubble injection and physically induced changes in solubility.

Below the mixed layer, where we do not have Ar data, we assume that Ar concentrations are at saturation for the calculation of $[O_2]^B$ (this assumption is evaluated in section 4.1.4). Since there is no similar inert analog for N_2O, we follow the recommendation of Cassar et al. (2014) and apply a thermal correction to surface measurements to account for solubility changes resulting from recent heat flux. Using this correction, mixed layer $[N_2O]^B$ is calculated as

$$[N_2O]^B = [N_2O]_{meas} - [N_2O]_{eq} - [N_2O]_{thermal}. \quad (5)$$

Here $[N_2O]_{thermal}$ is derived following the equation of Keeling and Shertz (1992), with kinetic corrections and delay as per Jin et al. (2007).

$$[N_2O]_{thermal} = \frac{1}{1.3} \cdot \left(-\frac{\partial [N_2O]_{eq}}{\partial T} \cdot \frac{Q}{c_p \cdot \rho} \cdot \frac{86,400\ s}{1\ day} \right) \cdot \frac{1}{k_{N_2O}} \quad (6)$$

The term in parentheses represents the thermally induced sea-to-air flux of N_2O (mmol N_2O m^{-2} d^{-1}). Rapid temperature changes cause a disequilibrium between observed surface N_2O and the saturation concentration. The thermally induced flux of N_2O should be equal to the disequilibrium concentration gradient, multiplied by the gas transfer velocity of N_2O. We thus divide the thermal flux by k_{N_2O} to obtain the concentration offset, $[N_2O]_{thermal}$, produced by solubility effects averaged over the period one half month before the measurement time. The negative operator in equation (6) converts the air-to-sea heat flux (Q, W m^{-2}, the sum of latent heat, sensible heat, longwave, and shortwave radiative fluxes) and positive heat capacity (c_p, J kg^{-1} C^{-1}; multiplied by sea surface density, ρ, kg m^{-3}) into a sea-to-air N_2O flux. Here Q and c_p were estimated as localized mean values over the mixed layer residence time of N_2O from NCPE/NCAR Reanalysis 1 surface flux (6 h resolution data retrieved from https://www.esrl.noaa.gov/psd/data/gridded/data.ncep.reanalysis.html; Kalnay et al., 1996) and Level 3 MODIS Aqua SST (1 day, 9 km resolution mean of 11 μ daytime and nighttime data retrieved from https://oceancolor.gsfc.nasa.gov/cgi/l3; NASA Goddard Space Flight Center, Ocean Ecology Laboratory, Ocean Biology Processing Group, 2014a, 2014b). Below the mixed layer, no thermal correction for N_2O is made in the calculation of $[N_2O]^B$ (i.e., $[N_2O]_{thermal} = 0$ in equation (5)).

The solubility equations of Garcia and Gordon (1992, 1993) and Weiss and Price (1980) were used to derive the saturation concentrations of O_2 and N_2O, respectively, from SST and sea surface salinity measurements. In these calculations, we accounted for changes in atmospheric N_2O concentrations using observations from Barrow, AK (data provided by the NOAA ESRL Global Monitoring Division HATS Network and retrieved from https://www.esrl.noaa.gov/gmd/dv/iadv/; Hall et al., 2007).

The vertical $[O_2]^B/[N_2O]^B$ gradient (hereafter referred to as the "supply ratio") represents the stoichiometry of vertical mixing, with respect to biological O_2 and N_2O. Cassar et al. (2014) used a discrete two-point slope ($\frac{\partial [O_2]^B}{\partial [N_2O]^B} = \frac{[O_2]^B_{deep} - [O_2]^B_{ML}}{[N_2O]^B_{deep} - [N_2O]^B_{ML}}$), based on end-members within (ML) and below (deep) the mixed layer. We found that this approach produced significant variability in our NCP correction (discussed in section 4.1.1). We thus utilized depth profile measurements to estimate the supply ratio from the slope of the $[O_2]^B$ versus $[N_2O]^B$ relationship in the water column from the base of the mixed layer to 150 m below (mld to mld + 150 m). The supply ratio was therefore characterized independently for each cruise as the slope through the respective pooled data set of all profile measurements in the 150 m below the mixed layer. A similar approach was previously used by Castro-Morales et al. (2013) and Manning et al. (2017) in estimating vertical fluxes from O_2 gradients. As discussed below (section 4.1.1), the magnitude of the NCP correction is sensitive to the approach used to estimate the supply ratio term but is largely insensitive to the depth of integration or the threshold criterion of the mixed layer depth (mld) estimate.

2.5. Calculations of Apparent Mixing Coefficients, K_{mix}

To validate the NCP corrections, we calculated an apparent mixing coefficient (K_{mix}, m^2 s^{-1}) based on the mixed layer N_2O budget. The coefficient represents all vertical advection, diffusion, and entrainment processes over the mixed layer N_2O residence time. Assuming steady state and that N_2O is produced only

below the euphotic zone (see section 4.1.2), the mixing coefficient is calculated from the surface N_2O mass balance as follows:

$$K_{mix} = \frac{k_{N_2O} \cdot [N_2O]^B}{\partial [N_2O]^B / \partial Z} \cdot \frac{1 \text{ day}}{86,400 \text{ s}}, \quad (7)$$

where $K_{mix} \cdot (\partial[N_2O]^B/\partial Z)$ is the vertical mixing flux of $[N_2O]^B$ (mmol m^{-2} s^{-1}) and $k_{N_2O} \cdot [N_2O]^B$ is the air-sea flux (mmol m^{-2} d^{-1}). The vertical gradient of $[N_2O]^B$, $\partial[N_2O]^B/\partial Z$ (mmol m^{-4}), was estimated at each station with profile N_2O measurements as the depth-dependent regression slope of all N_2O measurements in the 150 m below the mixed layer.

2.6. Ancillary Hydrographic Data and Calculations

Ancillary hydrographic data were collected and provided by the Institute of Ocean Sciences laboratory of the Department of Fisheries and Oceans Canada. Continuous underway measurements of SST and sea surface salinity were obtained from a thermosalinograph (*Sea-Bird* CTD *SBE-21*) connected to the ship's surface seawater supply. Depth profiles of temperature and salinity were obtained from CTD casts using a *Sea-Bird* CTD (*SBE-911-plus*) mounted on the Rosette frame. We used a density-difference criterion of 0.125 kg m^{-3} to define the mld.

Water column measurements of O_2 (at depths corresponding to our N_2O samples) were made by discrete Winkler titrations, using an automated titration system (*Metrohm Dosimat 876*) (Carpenter, 1965). Chlorophyll (chl) *a* samples, collected onto 25 mm GF/F filters prior to extraction in 90% acetone, were measured on a *Turner 10 AU* fluorometer before and after acidification to correct for phaeopigments (Welschmeyer, 1994). Nitrate and nitrite (NO_3^- + NO_2^-) samples were measured spectrophotometrically using an *Astoria* autoanalyzer (Barwell-Clarke & Whitney, 1996).

Higher-resolution (1 m depth intervals) O_2 measurements were made using a *SBE-43* O_2 sensor mounted on the CTD platform. These data were used to evaluate the gradient of biological O_2 ($\partial[O_2]^B/\partial Z$, mmol m^{-4}) below the mixed layer at each station along the Line P and La Perouse transects. The gradient was taken as the slope of the regression line through each station's data set in the 25 m interval below the mixed layer (i.e., $\partial[O_2]^B/\partial Z|_{25}$). We selected an integration depth of 25 m as it represents the depth range immediately below the mixed layer and the direct water source for vertical mixing to the surface. As we explain in section 4.1.5.1, we use these O_2 gradients to diagnose situations where the N_2O correction could not be applied.

3. Results

In the presentation of our results, we divide our sampling area into two distinct hydrographic regions, based on the spatial patterns we observed in NCP, chl *a*, and nutrient concentrations. The off-shelf region consists of those portions of the Line P transect west of station P4, while the on-shelf (coastal) region includes all of the La Perouse track, and the Line P transect east of and including P4. This separation corresponds approximately with the location of the continental slope (500–1,000 m isobaths; Figure 1) and is similar to previous divisions of the Line P transect (Whitney et al., 1998) and other physical representations of the continental shelf region (Crawford & Thomson, 1991). We first present our observations of hydrography and plankton biomass across these two regions (section 3.1). Then we examine the relationship between O_2 and N_2O and assess how N_2O data can be used to derive mixing coefficients to correct NCP estimates (sections 3.2 and 3.3). We finish by examining the spatial patterns of NCP across our survey region in relation to other oceanographic variables (section 3.4). Limitations of the N_2O correction approach are addressed in the discussion (section 4.1).

3.1. Hydrographic Conditions and Phytoplankton Biomass

During our cruises, the spatial and temporal variability in mixed layer chl *a* generally followed typical patterns for our study area, with the highest chl *a* in the on-shelf region (up to 38 mg m^{-3} during the August Line P cruise) and lower values (~0.2–0.8 mg m^{-3}) in much of the off-shelf region (Figures 2a–2c). We observed the expected seasonal cycle in surface chl *a* in the coastal waters, with values increasing from $<$1.2 mg m^{-3} in February to $>$10 mg m^{-3} in May and June, and $>$30 mg m^{-3} in August. In the off-shelf region, winter and spring concentrations (~0.2–0.8 mg m^{-3}) were usually greater than in August ($<$0.4 mg m^{-3} west of station P8). Peaks in chl *a* were observed near OSP during the spring and summer. The maximum chl concentration observed at OSP on the June cruise (1.2 mg m^{-3}) was unusually high (relative to the long-term summer average of ~0.4 mg m^{-3}).

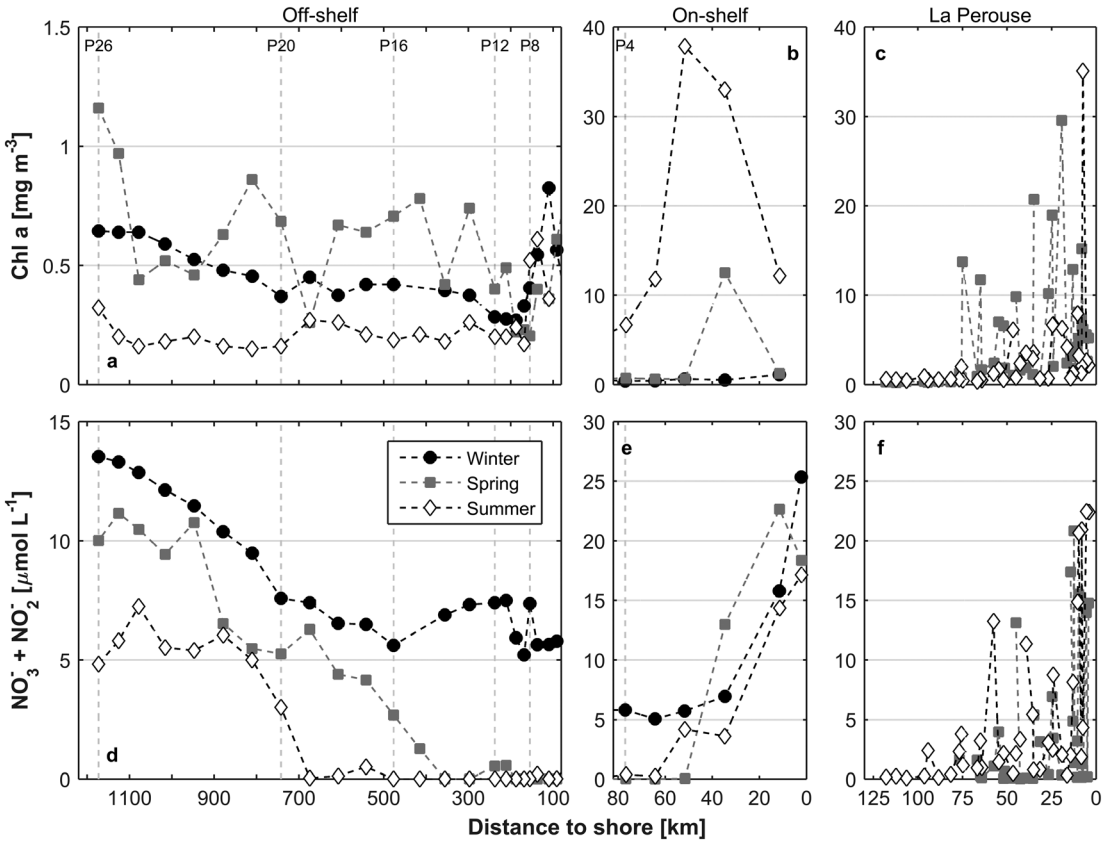

Figure 2. Mixed layer chl *a* (a–c) and $NO_3^- + NO_2^-$ (d–f) concentrations along the 2016 Line P and La Perouse transects. Data are separated into the off-shelf (a, d) and on-shelf (b, e) regions of the Line P transect and the La Perouse cruise (c, f). Note that the winter on-shelf symbols in Figure 2b are obscured behind the spring symbols and that the *x* and *y* scales differ among some of the panels.

Dissolved $NO_3^- + NO_2^-$ showed maximum concentrations (>10 μmol L^{-1}) closest to shore in all three seasons (Figures 2d–2f). In the oceanic waters, concentrations were highest in February, ranging from ~5 μmol L^{-1} at the boundary between the on-shelf and off-shelf zone (approximately 80 km from shore) to nearly 14 μmol L^{-1} at OSP (Figure 2d). June and August had a similar spatial pattern, but concentrations decreased through the spring and summer. In general, spring and summer nutrient concentrations in the southern shelf region were low to about 40 km off shelf (<6 μmol L^{-1}) but increased sharply toward the coast to values above 10 μmol L^{-1} (Figures 2e and 2f). Between stations P4 and P14 (~400 km from shore), we observed near depletion (<0.5 μmol L^{-1}) of mixed layer $NO_3^- + NO_2^-$ in June. In August, the off-shelf depletion extended to over 600 km. Beyond the regions of macronutrient depletion, concentrations increased but never reached maximum values observed in the winter. The elevated summer macronutrient concentrations in off-shelf waters are taken as evidence of Fe limitation (Varela & Harrison, 1999).

3.2. O_2 and N_2O

Depth profiles of O_2 and N_2O in the upper water column exhibited a linear relationship at all stations. Our measurements, made in 2016, are consistent with those from previous Line P and La Perouse cruises dating back to 2012 (Capelle & Tortell, 2016) (Figure 3a). Both O_2 and N_2O typically exhibited homogeneous distributions and supersaturation in the mixed layer ($[O_2]^B$ and $[N_2O]^B > 0$; surface $[N_2O]^B$ data are presented in Figure S2). With the exception of some off-shelf stations during spring and summer, N_2O supersaturation increased monotonically below the mixed layer, while O_2 became significantly undersaturated (Figures 3a and S3; deviations are discussed below in section 4.1.5.1). From all available profile data (2012 to present), we thus derived an inverse linear relationship between $[O_2]^B$ and $[N_2O]^B$, which yielded a narrow distribution in the subsurface-to-surface (mld to mld + 150 m) supply ratio terms (Figure 3b). Based on 2016 profile data, our calculated supply ratios ranged from -3.2×10^4 to -1.0×10^4 (mean -1.5×10^4) mmol O_2 (mmol N_2O)$^{-1}$.

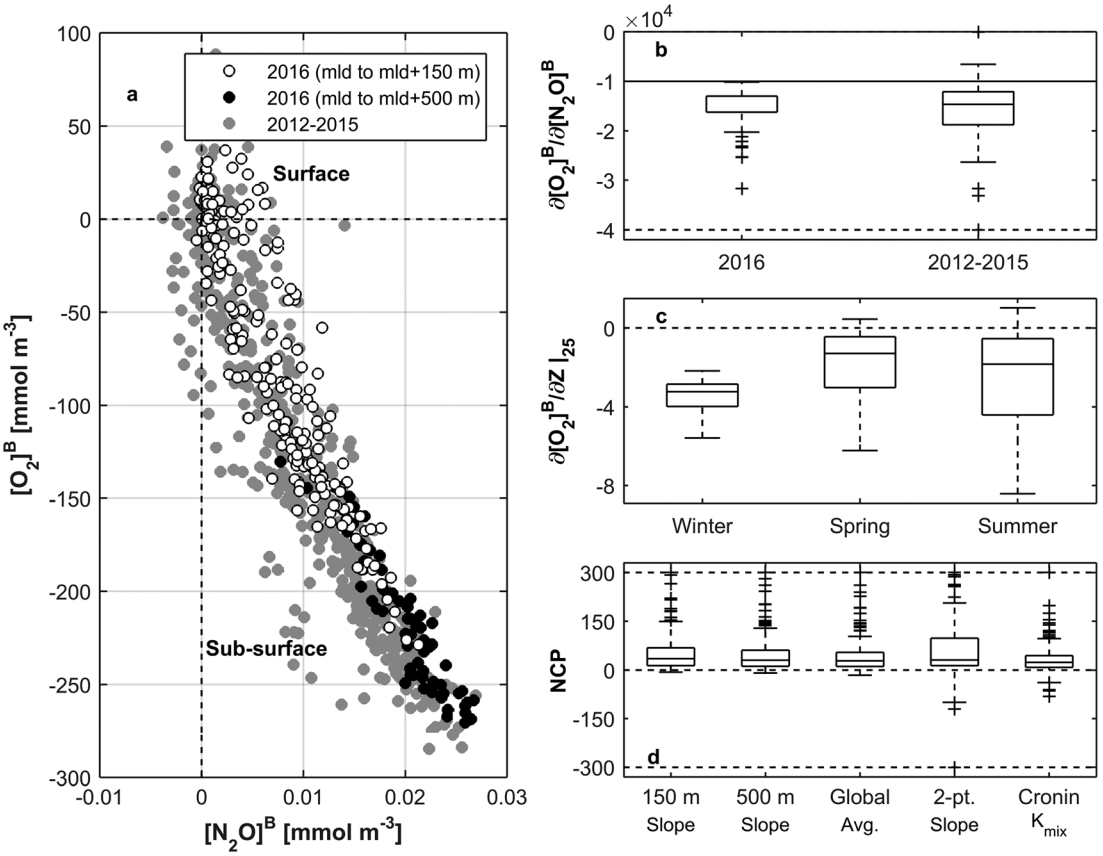

Figure 3. Relationship between N_2O and O_2 concentrations in the upper water column (a), showing $[N_2O]^B$ and $[O_2]^B$ from all 2016 measurements to 150 m (white) and 500 m (black) below the mixed layer, and previous observations to 500 m below the mixed layer (2012–2015, gray). The dashed lines indicate 100% saturation. (b) The distribution of supply ratio estimates derived from 2016 data only, and 2012–2015 data, calculated for each station in the 150 m below the mixed layer (see text for further explanation). The solid horizontal line denotes a slope of -1×10^4 mmol O_2 (mmol $N_2O)^{-1}$, representing the global approximate average stoichiometry of O_2/N_2O (e.g., Nevison et al., 2003). (c) Estimates of the subsurface $[O_2]^B$ gradient by season (2016 cruises only), defined in the 25 m below the mixed layer. The absolute sensitivity of NCP estimates to the supply ratio term, the method of estimating it, and the correction approach is shown in (d). Corrected NCP wasNCPestimated using a supply ratio derived in the 150 m below the mixed layer, 500 m below, using the global stoichiometric average value, and a two-point slope. We also evaluated NCP by making corrections using a literature-derived eddy diffusivity value and our estimates of $\partial[O_2]^B/\partial Z|_{25}$ (see section 4.1.5.2 for more details). In (b)–(d), the boxes show the 25th, 50th, and 75th percentile values (bottom, middle, and top lines, respectively). Whiskers extend to the 1st and 99th percentile ranges, and crosses represent outlying data beyond this range. The lower limit in (b) was restricted to -4×10^4 mmol O_2 (mmol $N_2O)^{-1}$, and the scale in (d) was limited to ±300 mmol O_2 m^{-2} d^{-1}.

These values fall well within the range we observed along Line P since 2012 (-1.2×10^5 to -6.6×10^3 mmol O_2 (mmol $N_2O)^{-1}$), with 99% of 2016 gradients being within one standard deviation of the 2012–2016 mean ($-1.8 \times 10^4 \pm 1.3 \times 10^4$ mmol O_2 (mmol $N_2O)^{-1}$).

Estimates of the $[O_2]^B$ gradient in the 25 m below the mixed layer ranged from -8.4 to 1.1 mmol O_2 m^{-4} (Figure 3c). Thus, at some stations, we observed increasing or near-constant $[O_2]^B$ concentrations below the mixed layer ($\partial[O_2]^B/\partial Z|_{25} \geq -0.1$). All of the positive values (i.e., higher O_2 concentrations below the mixed layer) occurred during the spring or summer in the off-shelf region. In contrast, only negative gradients were observed in the coastal regions during all seasons (Figure S4). Where N_2O profiles were obtained, we also observed N_2O deficits (i.e., $\partial[N_2O]^B/\partial Z|_{25} < 0$) coincident with the O_2 maxima and therefore linear negative $[O_2]^B/[N_2O]^B$ gradients with depth (Figure S3). The supply ratio for these profiles was not significantly different than the other stations or seasons.

3.3. Apparent Mixing Coefficients

Based on our N_2O measurements, we derived apparent mixing coefficients (representing all vertical advection, diffusion, and entrainment processes) between 1.1×10^{-4} and 1.7×10^{-3} (mean 6.7×10^{-4}) m^2 s^{-1} (Figure 4). Values are presented only where stations showed the expected negative O_2 gradient below the

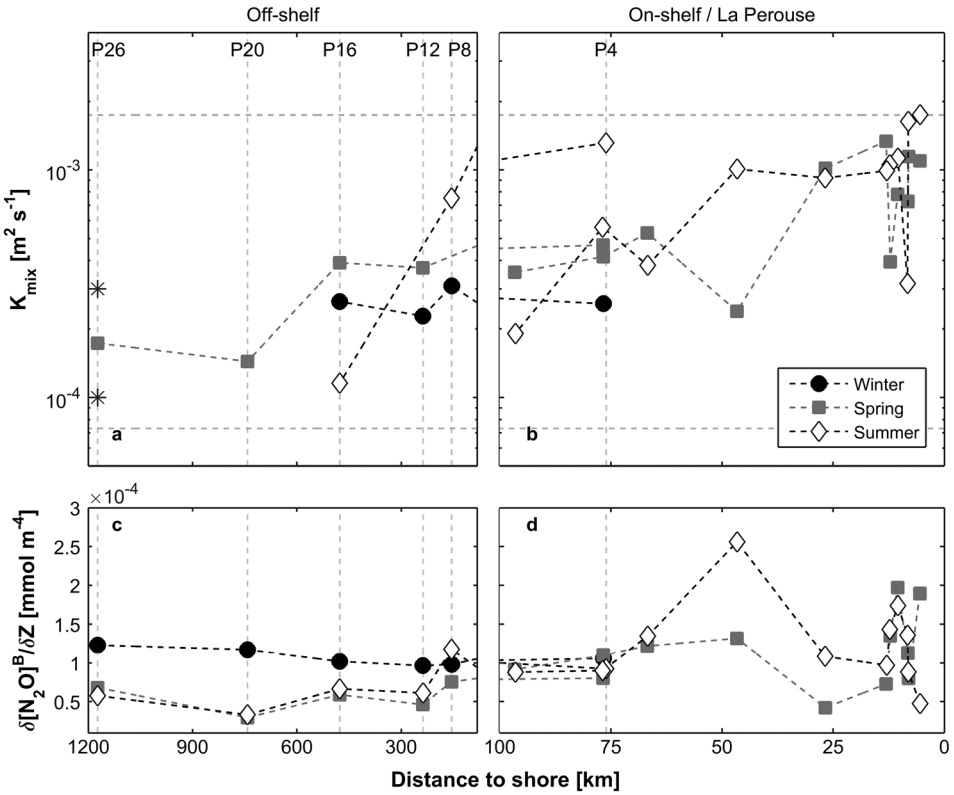

Figure 4. Vertical mixing coefficients derived from profile measurements of N_2O for the off- and on-shelf regions ((a) and (b), respectively). The asterisks in (a) represent the Ocean Station Papa (P26) summer and autumn mean eddy diffusivity (1×10^{-4} and 3×10^{-4} m^2 s^{-1}, respectively) estimated by Cronin et al. (2015). Note that our K_{mix} accounts for vertical diffusivity, advection, and entrainment fluxes, while these latter values do not include advection and entrainment. The horizontal dashed lines represent the upper and lower K_{mix} values after accounting for mixed layer nitrification (see section 4.1.2). The *y* axis in (a) and (b) is on a logarithmic scale. (c and d) The corresponding subsurface $[N_2O]^B$ gradients (derived in the 150 m below the mixed layer), which are used to estimate K_{mix}. Values in all panels are only presented for stations where we obtained profile measurements of N_2O; K_{mix} is shown only where the NCP correction was not biased by a subsurface maximum in O_2 concentrations (see section 4.1.5.1).

mixed layer (see sections 3.4 and 4.1.5.1). Similarly, we did not calculate a K_{mix} value at several stations where we observed undersaturated N_2O concentrations in the mixed layer (Figure S2).

The largest K_{mix} values were observed in the on-shelf regions following periods of intense spring and summer upwelling (mean 8.2×10^{-4} m^2 s^{-1}). By comparison, mixing coefficients were lower in most of the off-shelf region during the same seasons (mean 3.2×10^{-4} m^2 s^{-1}), except following periods of increased wind speed (e.g., P8 in August). In the winter, we observed mixed layer N_2O undersaturation at P20 and P26, resulting in derived $K_{mix} < 0$ that cannot be used to correct NCP estimates. Elsewhere off-shelf, K_{mix} had intermediate values in February (mean 2.7×10^{-4} m^2 s^{-1}) and the lowest value at the coastal P4 station (2.6×10^{-4} m^2 s^{-1}), relative to the other Line P cruises.

3.4. Net Community Production

Figure 5 shows the spatial distribution of NCP during the winter (a and b), spring (c–e), and summer (f–h) cruises, with and without the N_2O correction. We present both uncorrected and corrected estimates, noting that some of the corrected values are biased by subsaturated surface $[N_2O]^B$, or subsurface $[N_2O]^B$ deficits (and $[O_2]^B$ maxima), which yield (nonsensical) negative mixing terms (discussed below in section 4.1.5.1). Our final NCP estimates are thus compiled from a combination of corrected and uncorrected values, with uncorrected NCP selected for regions where the N_2O correction could not be applied. In total, the N_2O correction could not be applied at 19 out of 137 locations (<15% of data points). A summary of mean and standard deviation values for final NCP and the N_2O correction is presented in Table S1.

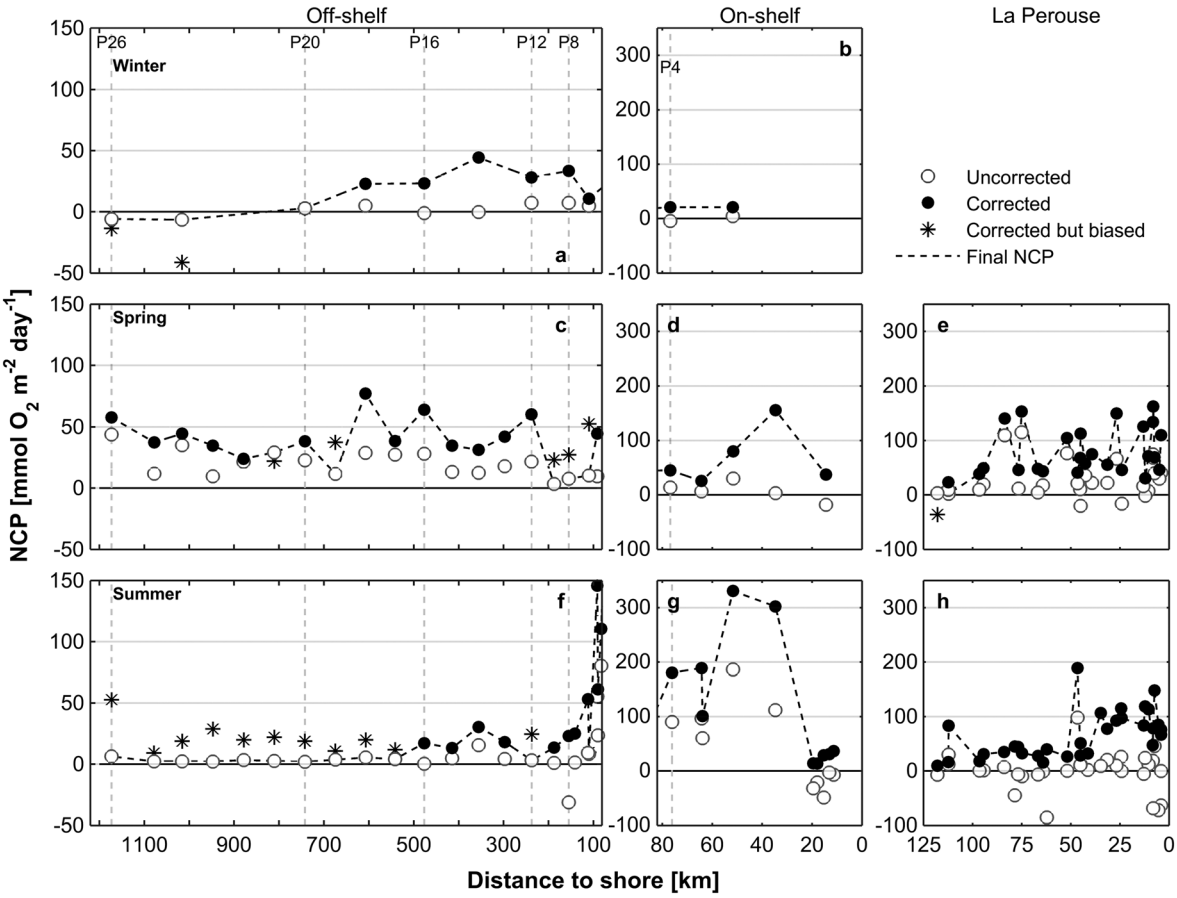

Figure 5. Uncorrected and corrected NCP estimates in winter (February Line P; a and b), spring (June Line P, c and d; May La Perouse; e), and summer (August Line P, f and g; September La Perouse, h). The dashed black lines trace our final NCP estimates, taken as the unbiased N_2O-corrected values (black markers) or uncorrected values (open-face markers) when corrected values were biased (asterisks). See text, section 4.1.5.1, for details of biased corrections. The Line P data are presented as the average of the outbound and inbound transects, and the La Perouse data show all stations arranged by their proximity to shore. The dashed vertical gray lines show the locations of major stations along Line P, while the solid horizontal line indicates 0 NCP. Note the difference in scale between the off-shelf (a, c, and f) and on-shelf regions (b, d, e, g, and h).

The N_2O correction always increased our estimated NCP over uncorrected values. The magnitude of the correction factor was generally highest in the on-shelf region during the summer, with an average of 75 mmol O_2 m^{-2} d^{-1} difference (3–190 mmol O_2 m^{-2} d^{-1} range) between corrected and uncorrected data. These corrections are equivalent to 23–327% of corrected NCP values. Prior to correction, several stations in the southern on-shelf region had negative NCP values in spring and summer, suggesting net heterotrophic conditions. After correction, however, all estimates became positive, implying net autotrophy. The absolute magnitude of the correction was lower in the off-shelf waters, with mean values of 23, 25, and 31 mmol O_2 m^{-2} d^{-1}, during the winter, spring, and summer respectively, but the relative contributions to corrected NCP were still high, (81, 52, and 74%, on average, respectively).

We observed negative NCP near OSP during the winter. However, the observation of undersaturated N_2O in the mixed layer at these stations meant that a correction could not be applied. True NCP here is likely higher than our uncorrected value, because our uncorrected value may be underestimated due to mixing of low-O_2 water from below (we discuss other correction approaches in section 4.1.5.2). In the spring, NCP was slightly higher at OSP relative to other oceanic stations, consistent with the coincident positive anomaly in chl *a* (Figure 2a).

Our final NCP shows a spatial gradient characterized by generally low values in the off-shelf region and highest values on shelf (Figures 5 and 6). For each spring and summer cruise, high NCP was observed in the southern WCVI area, with maximum values of 162, 182, 396, and 189 mmol O_2 m^{-2} d^{-1} in May, June, August, and

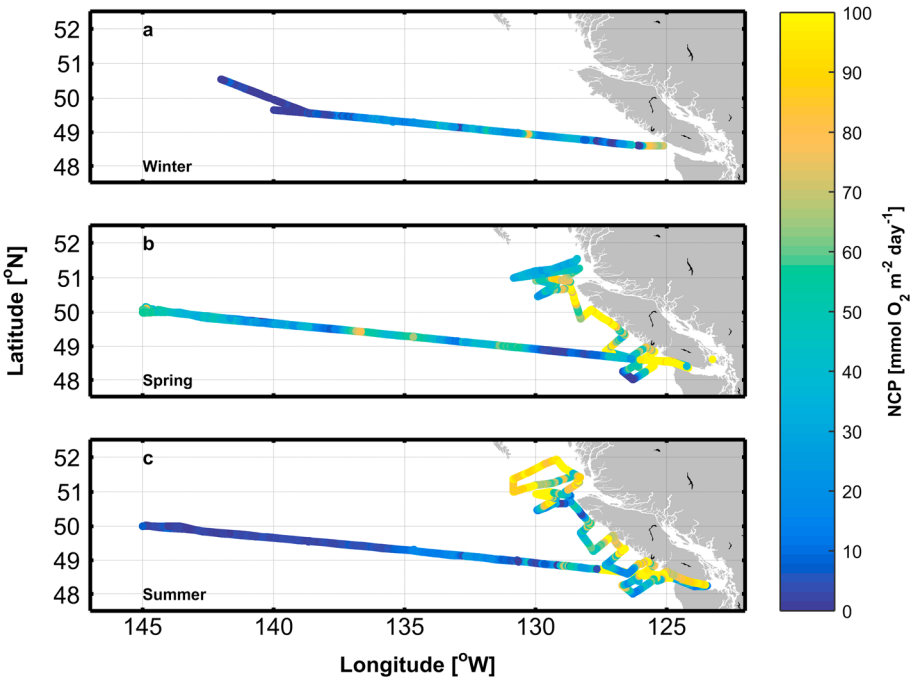

Figure 6. Spatial distribution of NCP in winter (a), spring (b), and summer (c), showing all outbound and inbound Line P data (overlaid). The N_2O correction was linearly interpolated to the resolution of our underway $\Delta O_2/Ar$ data.

September, respectively. Wintertime measurements in the same region revealed significantly lower NCP, at just ~24 mmol O_2 m^{-2} d^{-1} (maximum) and a weaker spatial gradient between coastal and oceanic stations. Our repeat sampling of this region suggests that NCP is persistently high over the on-shelf section of the Line P transect and between the LB and LC lines of the La Perouse survey during the spring and summer (Figure 6). The off-shelf extent of this high productivity region varies seasonally, with elevated NCP extending to ~50 km (126°W) from the coast in June and ~100 km of the coast (127°W) in August. Further north on the La Perouse track, we observed increased NCP on the transects adjacent to the coast (May; Figure 6b) and in Queen Charlotte Sound (September; Figure 6c). Off-shelf, during the spring and summer, NCP was mostly low, except for the high anomalies observed at OSP and between stations P16 and P20 in the spring. Relatively high NCP was also observed between P8 and P16 during the winter.

4. Discussion

To our knowledge, our work represents the first field application of the Cassar et al. (2014) method of N_2O-based corrections for $\Delta O_2/Ar$-derived NCP estimates. This approach is significant in enabling more robust productivity estimates in physically dynamic regions, where vertical mixing is a nonnegligible term in the mixed layer O_2 mass balance. Below, we discuss our results in terms of both methodological and practical considerations (section 4.1) and the interpretation of spatial and temporal patterns in NCP (section 4.3). In section 4.1.5, we outline some key limitations of, and alternatives to, the current approach and provide a discussion of uncertainties. The supporting information contains a detailed explanation of the uncertainties.

4.1. Methodological Considerations, Assumptions, and Limitations

We begin by addressing methodological considerations of the NCP correction, expanding on the work of Cassar et al. (2014), with emphasis on the implications for field studies. We focus on the use of different approaches to derive the O_2/N_2O supply ratio term, the possible impact of mixed layer nitrification, thermal solubility effects on mixed layer N_2O, and potential deviations from subsurface Ar saturation. We summarize by discussing the limitations of the current approach, outlining remaining uncertainties, and providing recommendations for future applications.

4.1.1. Considerations for the $[O_2]^B/[N_2O]^B$ Supply Ratio Term

Cassar et al. (2014) estimated the subsurface-to-surface supply ratio of O_2/N_2O based on a two-point slope, with end-members within and below the mixed layer. Using this approach, we obtained some supply ratio terms that resulted in unrealistic NCP values (<-300 or >400 mmol O_2 m^{-2} d^{-1}; Figure 3d) based on the range of previous estimates in our study area (see section 4.3). The two-point slope approach is highly sensitive to the selected depth of the end-members (i.e., the depth of discrete Niskin bottle sampling) and is thus susceptible to even minor irregularities in the profile data. For these reasons, we used an alternative approach, estimating the supply ratio as the multipoint slope through the pooled data sets of $[O_2]^B$ and $[N_2O]^B$ in the 150 m below the mld for each respective cruise.

The depth-dependent increase in $[N_2O]^B$ and corresponding decrease in $[O_2]^B$ that we observed at most stations yielded a narrow range of supply ratio estimates and is consistent with nitrification being the dominant source of N_2O in our study area (Capelle & Tortell, 2016; Grundle et al., 2012). Our supply ratio estimates are also consistent in space and time along the Line P and La Perouse transects, and the difference between vertical $[O_2]^B/[N_2O]^B$ gradients for individual profiles during a single cruise was not statistically significant. This result justifies the use of a pooled data set for each cruise. We selected an integration depth of 150 m as it extends fully beyond the maximum depths of the mixed layer and euphotic zone observed during the 2016 cruises, thereby capturing the subsurface regions of increased N_2O production. A similar depth of integration for vertical mixing (120 m) was used by Ianson and Allen (2002) in a physical model of the WCVI region.

The supply ratios derived by our multipoint slope approach did not produce any unrealistic negative NCP values (Figure 3d), and our estimates from the 2012–2016 data agree well with O_2/N_2O gradients reported in the region and with the global average of $\sim -1 \times 10^4$ mmol O_2 (mmol $N_2O)^{-1}$ (Cohen & Gordon, 1979; Nevison et al., 2003; Oudot et al., 1990; Rees et al., 1997). In the absence of depth profile data, a gradient of -1×10^4 mmol O_2 (mmol $N_2O)^{-1}$ may therefore constitute a suitable alternative in most regions. Indeed, we observed only small differences between NCP estimated using our data-derived supply ratio terms and the global average stoichiometric value (mean difference of 11.3 mmol O_2 m^{-2} d^{-1}; Figure 3d), with the largest deviations occurring in coastal waters with high surface $[N_2O]^B$ concentrations. Moreover, the NCP correction is generally insensitive to the depth of integration of the supply ratio term, provided that sufficient points are selected to accurately estimate a regression slope and that a region of subsurface nitrification is included (i.e., using integration depths that extend beyond the euphotic zone). When the gradient was estimated as the slope integrated over the 500 m below the mld, for example, we observed a mean deviation of 6.6 mmol O_2 m^{-2} d from our corrected NCP estimates (Figure 3d). Similarly, we found that varying our mld estimates by ±5 m resulted in less than 3.8% variation in the supply ratio terms (<1 mmol O_2 m^{-2} d^{-1} NCP). This demonstrates that our results are not overly sensitive to our choice of a 0.125 kg m^{-3} density difference criterion to define the base of the mixed layer. In all cases, the spatial patterns of NCP remain similar using different slope-derived supply ratio terms (data not shown), but the amplitude of the correction changes slightly. As we describe below in section 4.1.5, caution should nonetheless be exercised before applying the N_2O based approach in some scenarios.

4.1.2. Mixed Layer Nitrification

Nitrous oxide is produced mainly through nitrification, as a by-product of the oxidation of ammonium (AO) to NO_2^- and NO_3^- or through incomplete denitrification under low-O_2 conditions (Codispoti et al., 2005; Ward, 2000). It is believed that nitrification is photoinhibited in surface waters (Horrigan et al., 1981), while high mixed layer O_2 concentrations are not favorable for denitrification. The net result is that N_2O has typically been assumed to be produced mainly in subsurface waters (e.g., Dore & Karl, 1996), and this assumption is applied in the N_2O correction (equation (3)). Yet recent work suggests that N_2O production may occur within the euphotic zone (Grundle et al., 2013; Smith et al., 2014; Zamora & Oschlies, 2014). Cassar et al. (2014) suggested that mixed layer N_2O production would lead to an overestimate of the vertical mixing term and overcorrection of NCP. Below, we attempt to quantify the potential significance of this limitation.

During nitrification, $[N_2O]^B$ increases, while $\Delta O_2/Ar$ decreases as O_2 is consumed through AO. A similar net change occurs through mixing, such that the contribution of mixing, and subsequently the NCP correction, is overestimated when nitrification is neglected. We define NCP as net O_2 production resulting from gross photosynthesis, minus community respiration of organic carbon, such that only respiratory processes

affecting the organic carbon pool are considered. As such, nitrification is not an inherent component of our definition of NCP, and the NCP equation (equation (3)) can be adjusted, accounting for the effects of this process on both O_2 and N_2O (refer to the supporting information for the derivation).

$$NCP = k_{O_2} \cdot \left(\Delta O_2/Ar \cdot [O_2]_{eq} - \frac{k_{N_2O}}{k_{O_2}} \cdot \frac{\partial [O_2]^B}{\partial [N_2O]^B} \cdot [N_2O]^B \right) - N \cdot \left(1 - \frac{\Delta N_2O}{\Delta O_2} \cdot \frac{\partial [O_2]^B}{\partial [N_2O]^B} \right) \quad (8)$$

Here N is the nitrification rate in terms of O_2 consumption ($\leq$0 mmol O_2 m^{-2} d^{-1}), and $\frac{\Delta N_2O}{\Delta O_2}$ is the mixed layer N_2O stoichiometric yield of nitrification ($\leq$0 mmol N_2O (mmol O_2)$^{-1}$).

Applying equation (8), we calculate the potential impact of mixed layer nitrification on our 2016 NCP estimates, considering only those locations where the NCP correction was not biased (see section 4.1.5.1). Grundle et al. (2013) reported mean mixed layer nitrification rates of ~20 nM NH_4^+ d^{-1} along the off-shelf Line P transect, which is equivalent to O_2 consumption of 0.04 mmol O_2 m^{-3} d^{-1}, based on the stoichiometry of the reaction: $NH_4^+ + 2O_2 \rightarrow NO_3^- + H_2O + 2H^+$. Since rates of nitrification vary geographically, we use this regional value in our calculations (Table 1), recognizing that it falls within the range of globally reported rate estimates for near-surface waters (0–~130 nM NH_4^+ d^{-1}; Dore & Karl, 1996; Santoro et al., 2010; Ward, 2005). Based on 2016 mlds from our data, we derived mixed layer-integrated nitrification rates (N in equation (8)) between -0.4 and -3.6 mmol O_2 m^{-2} d^{-1}.

The impact of surface water nitrification on the N_2O correction approach depends on the N_2O yield of this process. The stoichiometric N_2O yield of nitrification ($\frac{\Delta N_2O}{\Delta O_2}$) varies widely under different substrate concentrations (Frame & Casciotti, 2010; Goreau et al., 1980) and will often differ from that of vertical mixing ($\frac{\partial [N_2O]^B}{\partial [O_2]^B}$; the reciprocal of the supply ratio). In the case where these two terms are the same, nitrification will have no net effect on the NCP correction, since equation (8) simplifies to equation (3). For the other (more likely) scenario, we can derive lower and upper bounds on our calculations, using low (-1.4×10^{-4} mol N_2O (mol O_2)$^{-1}$; Yoshida et al., 1989) and high (-3.8×10^{-4} mol N_2O (mol O_2)$^{-1}$; Santoro et al., 2011) N_2O yields reported under O_2 and NO_2^- concentrations similar to those observed in our study area.

The results of our calculations show that nitrification could produce between 0.04 and 0.26 μmol m^{-3} N_2O in the mixed layer, which is equivalent to 0.4–2.2% of mean 2016 surface concentrations (Table 1). These values translate into net reductions of NCP between 0.3 and 11.2 mmol O_2 m^{-2} d^{-1}, through the combined influence of altered O_2 and N_2O concentrations. On one hand, nitrification acts to decrease apparent NCP by consuming O_2 (equation (3)). Conversely, nitrification increases the surface N_2O saturation anomaly, thereby leading to an overestimate of the mixing correction term (i.e., leading to overcorrection of NCP). In our calculations, we found that nitrification would increase NCP by between 0.4 to 3.6 mmol O_2 m^{-2} d^{-1} through its effects on surface O_2 and decrease NCP by between 0.8 and 14.9 mmol O_2 m^{-2} d^{-1} through increased N_2O. These independent effects sum to produce the net influence on NCP (presented in Table 1). Similarly, K_{mix} (equation (S1)) could be between 0.7 and 58% lower than values calculated without consideration of nitrification (Figure 4).

We thus conclude that the effect of nitrification on NCP estimates could be substantial in our study region under conditions where background NCP and mixing rates are low (e.g., in open-ocean waters). Indeed, at the upper limit, the bias in NCP derived from mixed layer nitrification could be as much as 42% of the apparent NCP. By comparison, in productive coastal waters, the effect of surface nitrification tends to introduce only a small error (<4% in spring and summer). Direct observations of nitrification rates are required to better constrain the influence of this process on surface NCP estimates. In the absence of such data, we continue to support the assumption made by Cassar et al. (2014), since the uncertainty estimated here (mean 5.5 mmol O_2 m^{-2} d^{-1}, or 16% of estimated NCP based on high N_2O yields) is of similar magnitude and typically smaller than errors in the gas transfer parameterizations (mean 4.4 mmol O_2 m^{-2} d^{-1}; see the supporting information). We note, however, that NCP measurements made by this approach may still constitute an upper bound on true values.

4.1.3. Thermal Correction for $[N_2O]^B$

Following Cassar et al. (2014), we applied a thermal adjustment to mixed layer measurements of $[N_2O]^B$ (equations (5) and (6)) to account for solubility effects. Recent warming (cooling) prior to sampling

Global Biogeochemical Cycles

10.1002/2017GB005792

Table 1
The Potential Effects of Surface Nitrification on Mixed Layer N_2O Concentrations, NCP Estimates (ΔNCP), and Mixing Coefficients (ΔK_{mix})

		2016 data					Calculations						
		mld	τ	Mean N_2O	$\frac{\partial[O_2]^B}{\partial[N_2O]^B}$	$\frac{\partial[N_2O]^B}{\partial Z}$	Mixed layer nitrification rate	N_2O produced		ΔNCP		ΔK_{mix}	
Region		(m)	(days)	(μmol m^{-3})	(mmol $mmol^{-1}$)	(mmol m^{-4})	(mmol O_2 m^{-2} d^{-1})	(μmol m^{-3})	(%)	(mmol O_2 m^{-2} d^{-1})	(%)	(m^2 s^{-1})	(%)
Winter	Off	90.5	16.5	11.95	-1.08×10^4	1.07×10^{-4}	−3.6	0.09	0.7	−1.7	−6.2	-5.3×10^{-5}	−20.5
								0.25	2.1	−11.2	−41.9	-1.5×10^{-4}	−57.8
	On	69.0	16.3	11.47			−2.8	0.09	0.8	−1.3	−6.1	-4.0×10^{-5}	−15.6
								0.25	2.2	−8.6	−41.1	-1.1×10^{-4}	−43.9
Spring	Off	28.1	10.8	10.78	-1.40×10^4	9.55×10^{-5}	−1.1	0.06	0.5	−1.0	−2.2	-1.8×10^{-5}	−7.3
								0.16	1.5	−4.9	−10.7	-5.2×10^{-5}	−20.5
	On	14.1	8.8	12.79			−0.6	0.05	0.4	−0.5	−0.7	-9.2×10^{-6}	−1.3
								0.13	1.0	−2.4	−3.4	-2.6×10^{-5}	−3.7
Summer	Off	25.5	8.3	9.40	-1.29×10^4	1.05×10^{-4}	−1.0	0.04	0.5	−0.8	−1.7	-1.5×10^{-5}	−4.3
								0.13	1.3	−4.0	−9.2	-4.3×10^{-5}	−12.1
	On	10.9	16.8	16.15			−0.4	0.09	0.6	−0.3	−0.3	-6.5×10^{-6}	−0.7
								0.26	1.6	−1.7	−1.6	-1.8×10^{-5}	−1.9

Note. We estimated the proportional contribution of in situ nitrification to surface N_2O concentrations (N_2O produced) based on literature-derived values of mean ammonium oxidation rates and N_2O yields of nitrification (see text for details). The effects on NCP and K_{mix} were estimated following equations (8) and (S1). Mixed layer depths and N_2O residence times (τ) represent the average values for the off-shelf and on-shelf regions, respectively, in each season. The two rows of calculations for each region represent values based on the low (shaded gray) and high N_2O yield estimates, respectively. Percent values (%) represent the proportional change in a variable relative to values estimated when nitrification was neglected.

Table 2
Influence of Air-Sea Heat Flux (Q, Equation (6) on Mixed Layer N_2O Budgets During One Residence Time of N_2O Prior to Sampling

Region		Air-sea heat flux ($W\ m^{-2}$)	Sea-air thermal N_2O flux ($\mu mol\ m^{-2}\ d^{-1}$)	ΔNCP ($mmol\ O_2\ m^{-2}\ d^{-1}$)	ΔNCP (%)
Winter	Off	−18.8	−0.13	−1.4	−5.3
	On	−17.0	−0.11	−1.2	−5.6
Spring	Off	126.7	0.75	11.4	25.2
	On	110.3	0.61	8.2	11.6
Summer	Off	120.4	0.57	7.8	18.3
	On	123.6	0.65	8.0	7.5

Note. The effect of thermally derived N_2O changes on NCP was estimated by comparing calculations with and without the thermal N_2O correction (ΔNCP represents the change in NCP if the thermal adjustment is not made). Negative heat fluxes represent ocean cooling, which induce negative sea-air N_2O fluxes according to equation (6).

decreases (increases) N_2O solubility and increases (decreases) the apparent saturation anomaly, causing a N_2O efflux (influx) at the surface. Since the residence time of gases in the mixed layer is typically 2–3 weeks, atmospheric gas exchange lags behind changes in gas solubility. As a result of warming (cooling), mixed layer $[N_2O]^B$ would appear oversaturated (undersaturated), and the NCP correction would be too large (small). Figure S2 shows $[N_2O]^B$ with and without the thermal adjustment, and the resulting effect on NCP is proportional to the difference in observed concentrations. Using our unbiased corrected NCP, we find that the effect of the N_2O thermal correction is generally small in absolute magnitude (<11.4 mmol O_2 m^{-2} d^{-1}) but proportionately large (up to 25%), in low productivity, off-shelf regions (Table 2). For air-sea heat fluxes exceeding 100 W m^{-2} in magnitude (spring and summer), estimated NCP would be more than 7.8 mmol O_2 m^{-2} d higher in the absence of thermal adjustment. When NCP is relatively low, as in much of the off-shelf regions, such large heat fluxes can contribute >20% bias in final NCP estimates. We thus recommend the continued application of this correction for NCP estimates in off-shelf waters, despite the relatively large errors associated with estimates of surface heat fluxes (see the supporting information Table S2). By comparison, the thermal correction makes a relatively small (mean ~9%) contribution to the overall uncertainty in coastal NCP, due to the large magnitude of NCP estimates here but should still be included since thermal fluxes are likely to vary widely in space and time.

4.1.4. Ar Saturation Below the Mixed Layer

In the calculation of the vertical $[O_2]^B$ term, the NCP correction approach assumes that subsurface Ar concentrations are at saturation. Departures from this impact the derived supply-ratio term. Recent work in the North Pacific by Hamme and Emerson (2002) and Emerson et al. (2012) suggests that subsurface Ar concentrations rarely deviate from saturation by more than ±4%. In the absence of corresponding profile measurements of Ar, we recalculated all supply ratio terms, assuming ΔAr = ±0.04, to estimate the upper limit on the potential uncertainty in $\frac{\partial[O_2]^B}{\partial[N_2O]^B}$. We found that gradients were up to 3.2% steeper (shallower) when Ar was supersaturated (undersaturated). This source of error is small compared with the larger uncertainties in the gas transfer velocity parameterization and supply ratio terms (see the supporting information), and we thus suggest that deviations in Ar from equilibrium can be neglected without a significant influence on the overall results.

4.1.5. Discussion of the Approach Limitations and Uncertainties

4.1.5.1. Scenarios Where the N_2O Correction Approach Is Invalid

There are several scenarios for which NCP corrections based on the O_2/N_2O supply ratio may not be suitable. In much of the Arctic Ocean, for example, a complex N-cycle (Brown et al., 2015) and lack of a consistent relationship between O_2 and N_2O (Fenwick et al., 2017) invalidate this approach and likely preclude the use of N_2O corrections. Furthermore, regions where the subsurface $[O_2]^B/[N_2O]^B$ supply ratio does not represent the relevant gradient for vertical O_2 mixing pose a limitation to the correction approach of Cassar et al. (2014). Principally, this occurs under situations where subsurface O_2 maxima cooccur with localized minima in N_2O and a negative relationship between $[O_2]^B$ and $[N_2O]^B$ persists. Here the intuitive NCP correction should be to lower uncorrected values, since the upward supply of relatively high-O_2 water from beneath the mixed layer would introduce a positive $\Delta O_2/Ar$ anomaly. However, since the supply ratio stoichiometry of $[O_2]^B/[N_2O]^B$ remains negative, a false positive correction term is derived (i.e., corrected NCP > uncorrected NCP), leading to an overestimation of NCP, if equation (3) is applied. We observed this "biased" scenario at a number of off-shelf stations in June and August and chose to present uncorrected data for these regions in the absence of a suitable correction factor (see section 4.1.5.2 below). The same limitation would also occur in regions where $[N_2O]^B$ and $[O_2]^B$ both decline below the mixed layer ($\partial[O_2]^B/\partial[N_2O]^B > 0$), as might be seen where near-surface oxygen minimum zones result in N_2O loss through denitrification (e.g., Farías et al., 2009). In these cases, the positive supply ratio would yield a negative correction term, even though vertical mixing would have introduced a low-$\Delta O_2/Ar$ anomaly.

It is thus evident that the NCP approach applied here is invalidated if N_2O decreases below the mixed layer. In general, the approach works well when subsurface $[N_2O]^B$ increases, and $[O_2]^B$ decreases, as was the case at all coastal stations (where we found the largest correction terms) and much of the off-shelf region. Yet our extensive O_2 and N_2O profile measurements show that the approach, as described by Cassar et al. (2014), is not likely to be valid everywhere. At several stations, we observed deficits in subsurface N_2O that corresponded with relative maxima in O_2 (e.g., Figure S3). Although we lack profile measurements of N_2O at every sampling station, we can utilize our CTD-derived O_2 measurements to diagnose this limitation. By independently evaluating the depth-dependent O_2 slope in the 25 m below the mixed layer ($\partial[O_2]^B/\partial Z|_{25}$) in every profile, we observed a number of stations with positive gradients in the off-shelf region during the spring and summer (Figures 3 and S4). Where profiles of N_2O existed, corresponding deficits in N_2O, resulted in a negative O_2/N_2O gradient that was not significantly different than all other stations (Figure S3e). The observation of a consistent negative supply ratio term in all profile data resulted in positive correction terms, and overestimation (i.e., positive bias) of true NCP when the N_2O-based approach was used.

It is important to note that the O_2 minima/N_2O maxima that we describe here are shallow features, localized to the waters just below the mixed layer (Figure S3). Beyond these depths, we typically observe declining O_2 and increasing N_2O concentrations. For this reason, the $\partial[N_2O]^B/\partial Z$ values we use to derive K_{mix} terms (integrated down to 150 m below the mixed layer) are not explicitly negative for the regions where the NCP correction is biased (Figures 4c and 4d). We simply lack the depth resolution of N_2O measurements to better constrain the relevant slope over a shallower depth range. We find the presence of these N_2O minima to be somewhat counterintuitive and difficult to explain, since O_2 concentrations are clearly high enough to prevent N_2O loss through denitrification.

Finally, we also note that the current approach breaks down at other stations where mixed layer N_2O is undersaturated ($[N_2O]^B < 0$; e.g., P20–P26 in February). This scenario results in a nonsensical negative mixing correction term.

We therefore suggest that stations that do not exhibit significantly negative subsurface $[O_2]^B$ gradients, or where surface N_2O is undersaturated, should be precluded from the $[O_2]^B/[N_2O]^B$ supply ratio-based NCP correction. We use an upper $\partial[O_2]^B/\partial Z|_{25}$ cutoff threshold of -0.1 mmol O_2 m^{-4} (Figure S4) as mixing fluxes using this value are small (<4 mmol O_2 m^{-2} d^{-1}) for the mixing rates we observe off shelf. If O_2 profiles are not available to diagnose the suitability of the N_2O correction, this limitation may apply in oceanic regions with strong density stratification and deep euphotic zones, where subsurface primary productivity may generate an O_2 maximum or when water masses containing signatures of high productivity are subducted beneath surface layers. This scenario is prevalent in much of the North (tropical to midlatitude) Pacific during the summer time (Shulenberger & Reid, 1981). Yet strong density stratification in these regions will likely act to minimize the impact of vertical mixing fluxes, thus limiting the potential importance of NCP corrections (Giesbrecht et al., 2012). Nonetheless, future studies should focus on O_2 and N_2O dynamics in these waters, to understand the cause of subsurface N_2O deficits and to evaluate whether N_2O-based corrections could be feasible.

4.1.5.2. Alternatives to the N_2O Correction Approach

As an alternative to the N_2O approach, a correction can be made using estimates of a mixing rate and observed subsurface O_2 gradients (i.e., $-K_{mix} \cdot \partial[O_2]^B/\partial Z$). When we apply this correction to our data using average off-shelf K_{mix} values for the respective seasons, we obtained correction terms exceeding 75 mmol O_2 m^{-2} d^{-1} at stations P20–P26 in February and final NCP of ~50 mmol O_2 m^{-2} d^{-1}. These elevated NCP values are more than twofold higher than previous estimates (e.g., Giesbrecht et al., 2012; Palevsky et al., 2016; Yang et al., 2017). We therefore believe these values to be the unrealistic result of a combination of very strong subsurface O_2 gradients and overestimation of K_{mix} using the off-shelf (station P8–P16) average value. Indeed, the subsurface $[N_2O]^B$ gradients at stations P20 and P26 were steeper than at the other off-shelf stations (Figure 4c), such that the K_{mix} terms are likely to be smaller than predicted by the average value. Similarly, off-shelf $\partial[N_2O]^B/\partial Z$ differs between stations in the summer, and average K_{mix} values may be a poor representation of the regional mixing rates.

Our study clearly demonstrates the spatial and temporal variability of oceanic mixing rates (Figure 4). We thus caution against the use of non-site-specific and literature-derived estimates of K_{mix} or eddy diffusivity when

deriving NCP corrections. To examine the sensitivity of estimates to the choice of mixing rates used for correction, we recalculated corrected NCP using the mean summertime eddy diffusivity value of Cronin et al. (2015) (1×10^{-4} m^2 s^{-1}) and our independent subsurface O_2 gradient estimates (Figure 3d). On average, these estimates differed from our N_2O-corrected values by 32.4 mmol O_2 m^{-2} d^{-1} (~50% mean). This result underscores the importance of independent estimates of mixing rates for each respective station. In the absence of such direct estimates, we suggest the use of uncorrected NCP as the most viable option at present. This seems reasonable given the low apparent contribution of mixing fluxes to surface $\Delta O_2/Ar$ in the summertime (Giesbrecht et al., 2012; Palevsky et al., 2016; Yang et al., 2017). In coastal regions, where mixing corrections are largest, the O_2 and N_2O profiles permit the use of the N_2O-based correction approach. In summary, our analyses highlight the importance of examining the shape of the O_2 profiles before applying the N_2O-based NCP correction.

4.1.5.3. Additional Limitations of In Situ NCP Estimates

Additional limitations and uncertainties (see section S2 for a detailed error analysis) of the present approach are inherent to the majority of ship-based estimates of NCP from surface $\Delta O_2/Ar$ measurements. Specifically, NCP derived from O_2 mass balance equations (equations (1) and (3)) assumes steady state of surface O_2 concentrations and negligible horizontal fluxes. The present approach provides corrections for vertical mixing (diffusion, entrainment, and advection) but makes no attempt to rectify potential fluxes from these additional sources.

In a Southern Ocean Lagrangian study, Hamme et al. (2012) observed absolute changes in $\Delta O_2/Ar$ up to 0.6%, partially attributable to diurnal cycles in productivity. We found that $\Delta O_2/Ar$ varied by 3% (from ~3.5 to 6.5%) during a 1 day occupation of OSP in June, with lower variability (mean 0.1% d^{-1} off-shelf and 0.5% d^{-1} on-shelf; overall maximum 2.5% d^{-1}) observed between outbound and inbound sampling of the same locations along the Line P cruises. Thus, while the timing of our sampling (i.e., during the diel cycles) has an effect on the magnitude of our $\Delta O_2/Ar$ measurements, the uncertainty in NCP attributed to temporal changes in $\Delta O_2/Ar$ (~0.6 and 1.1 mmol O_2 m^{-2} d^{-1} off-shelf and on-shelf, respectively) is smaller than errors associated with gas flux parametrizations (~4.4 mmol O_2 m^{-2} d^{-1}).

Off-shore, lateral advection is likely to be negligible, but near the coast, a combination of high current speeds and patchiness in phytoplankton biomass may make horizontal fluxes significant. Using net current velocity data (data provided by the NASA Physical Oceanography Distributed Active Archive Center and retrieved from https://doi.org/10.5067/OSCAR-03D01; Bonjean & Lagerloef, 2002; Earth Space Research, 2009) and derived estimates of the surface lateral $[O_2]^B$ gradient (from our underway $\Delta O_2/Ar$ and thermosalinograph data), we estimated mean horizontal fluxes of ~1.6 and 22.7 mmol O_2 m^{-2} d^{-1} off-shelf and on-shelf, respectively. This level of uncertainty applies to measurements of NCP in Eulerian studies. However, in a Lagrangian sense, lateral advection influences the location assigned to a given NCP measurement but not the rate itself, so these flux estimates are in many cases an exaggeration of the influence of lateral advection on NCP rates.

Finally, the relatively low spatial resolution of our surface N_2O measurements (mean of 102, 37, and 47 km in our winter, spring, and summer cruises respectively) also limits the application of this approach on highly resolved space scales. We obtained estimates of NCP on the sub-kilometer scale (as in Figure 6) by linearly interpolating the N_2O correction term to the resolution of our underway $\Delta O_2/Ar$ measurements. However, we estimate a mean uncertainty in these values of 5.5 mmol O_2 m^{-2} d^{-1} by comparing estimates derived through linear and nearest-neighbor interpolation schemes (see the supporting information for more details). This additional uncertainty motivates the need for improved resolution of N_2O measurements. Our comparison between samples obtained from Niskin and the ship's seawater supply (Figure S1) shows that high quality N_2O measurements can be derived without the need for discrete, on-station bottle sampling, suggesting good possibilities for continuous underway analysis. Nitrous oxide measurements are not common on most oceanographic field programs, and existing data are largely based on discrete sampling. However, recent developments in instrumentation (Arévalo-Martínez et al., 2013; Grefe & Kaiser, 2014) should provide additional impetus for the development of ship-based underway N_2O measurements to complement mass spectrometry-based $\Delta O_2/Ar$ data. This would constitute an important next step in the application of the correction approach, enabling sub-kilometer spatial resolution of N_2O-corrected NCP estimates.

Overall, in spite of the above mentioned limitations and uncertainties, the N_2O approach we evaluate here represents an improvement over existing techniques for evaluating NCP from ship-based measurements of $\Delta O_2/Ar$. Specifically, the total mean analytical and parameterization uncertainty in our data is 9.2 mmol O_2 m^{-2} d^{-1} (~34 and 21% of off- and on-shelf estimates), with the correction factor contributing roughly 4.3 and 13.7 mmol O_2 m^{-2} d^{-1} in each region (Table S2). Although the methodological uncertainties are large in some cases (combined maximum of ~16 and 26 mmol O_2 m^{-2} d^{-1} off-shelf and on-shelf), these represent conservative estimates. Moving forward, constraining the rate of upper ocean N_2O production, improving reanalysis products for the estimation of oceanic heat flux, and reconciling surface measurements of $\Delta O_2/Ar$ for lateral advection would significantly improve confidence in N_2O-derived vertical mixing correction terms, making this an important tool for resolving spatial and temporal patterns in NCP.

4.2. Correction Factor and K_{mix}

Previous studies that have corrected for mixing processes on the mixed layer O_2 mass balance have used literature values for eddy diffusivity coefficients (e.g., Bushinsky & Emerson, 2015; Weeding & Trull, 2014). These indirectly obtained values may obscure potentially significant variability in both space and time (see section 4.1.5.2). Moreover, these corrections only represent diffusive fluxes, such that additional means of quantifying advection or entrainment are required. This introduces additional uncertainty to the estimated mixing terms. Some approaches have relied on model-derived mixing fluxes to evaluate all three terms (e.g., Plant et al., 2016). Our approach does so empirically.

In general, the magnitude of K_{mix} (Figure 4) reflects regional and temporal differences in upwelling, water column stratification, and wind-induced mixed layer turbulence. We observed the largest apparent mixing coefficients (and NCP correction factors) in the on-shelf region following periods of upwelling (based on Bakun Upwelling Index values at 48°N, 125°W and 50°N, 131°W provided by the Pacific Fisheries Environmental Laboratory and retrieved from http://www.pfeg.noaa.gov/products/PFEL/modeled/indices/upwelling/NA/data_download.html; Bakun, 1973). Indeed, our mean on-shelf K_{mix} values strongly correlate with the regional upwelling index (R^2 = 63%; Figure S5). This result, and the occurrence of elevated on-shelf surface $[N_2O]^B$ concentrations during the spring and summer upwelling periods (Figure S2), is supported by previous observations showing that upwelling is the dominant N_2O transport process over the continental shelf along the WCVI (Capelle & Tortell, 2016). Strong stratification in off-shelf regions, resulting from high solar radiation and mixed layer shoaling, is likely responsible for the smaller mixing fluxes and coefficients in this region, during the summer. Higher winter and spring K_{mix} at the off-shelf stations, relative to summer, is likely due to increased wind speed (Figures S6a–S6c), which is directly relatable to the strength of eddy turbulence and Ekman pumping (Kundu et al., 2012). The relative decline in K_{mix} from P12 to P26 in the spring is mostly attributed to reduced wind intensities along the same gradient. Although wind speeds are highest during the winter, strong temperature stratification, caused by the persistent thermocline located just below the mixed layer at this time of year (data not shown), resists particularly large mixing rates. The low winter-time K_{mix} values at the coastal Line P station, P4, reflects the net downwelling that occurs during this time (Figure S5a). The observation of undersaturated N_2O in the winter waters at OSP and profiles with negative N_2O gradients (positive O_2 gradients) in the spring and summer makes it difficult to estimate mixing at some locations.

Overall, our estimates of K_{mix} are consistent with the multiyear OSP time series of Cronin et al. (2015), who used heat and salt budgets to estimate vertical diffusivities. The results of their work suggest an annual range of mixing rates from ~1×10^{-5} to 1×10^{-2} m^2 s^{-1}. Our derived estimates, based on N_2O observations (with and without considerations for potential mixed layer nitrification), are fully encompassed in the range reported by Cronin et al., as well as the direct depth-resolved measurements of eddy diffusivity at OSP (~1×10^{-5} –1×10^{-3} m^2 s^{-1} below the mixed layer) of Rousseau et al. (2010). Our K_{mix} values also show reasonable seasonal and spatial patterns. The increase in mixing coefficients closer to shore (in spring and summer) fits the global data set of Whalen et al. (2012), who identified elevated mixing rates over rough bottom topography, and near the coast. Indeed, the on-shelf WCVI region is characterized by heterogeneous bottom topography, with numerous canyons, that can result in intensified mixing (Allen & Durrieu de Madron, 2009). This result indicates that the N_2O correction approach can provide significant insight into physical processes occurring in near-surface ocean waters.

It is important to note that our K_{mix} represent the combined fluxes due to diffusion, advection, and entrainment, whereas other estimates typically express mixing rates in terms of diffusivity coefficients. While we do not evaluate the relative contributions of each process to the total vertical flux, others (e.g., Yang et al., 2017) have shown that vertical diffusivity dominates over entrainment or advection in the off-shelf waters. In coastal waters, during upwelling events, however, vertical advection is likely to play a considerable role. It is therefore understandable that our K_{mix} values are comparable to, but on the upper range of, values derived from other data sets, particularly in regions impacted by upwelling, or subject to significant entrainment.

4.3. Spatial Patterns of NCP

Our data contribute to our knowledge of NCP in the Subarctic Pacific by providing refined estimates across broad spatial scales and contrasting oceanographic regimes. Much of our understanding of NCP in the Subarctic NE Pacific comes from previous studies in the vicinity of OSP (Bushinsky & Emerson, 2015; Fassbender et al., 2016; Howard et al., 2010; Lockwood et al., 2012; Palevsky et al., 2016; Plant et al., 2016) or at discrete locations along the Line P transect (Giesbrecht et al., 2012; Hamme et al., 2010). By comparison, fewer studies have quantified NCP in the coastal regions of the Subarctic Pacific, owing to the difficulties in constraining vertical mixing fluxes (e.g., Jonsson et al., 2013), limiting our understanding of this ecologically significant regime. Here we compare our corrected NCP estimates to values reported elsewhere along the Line P transect and discuss the apparent spatial patterns in the context of observed biological and physical forcing.

Our NCP estimates for the oceanic regions are consistent with those previously derived from a mixed layer O_2 mass balance approach in the Subarctic Pacific, but the upper range of our values exceeds any previous estimates (~50, 81, and 180 mmol O_2 m^{-2} d^{-1} in winter, spring, and summer, respectively). At OSP, for example, previous spring and summer O_2-based NCP estimates have ranged from ~−10 to 60 mmol O_2 m^{-2} d^{-1} (Bushinsky & Emerson, 2015; Fassbender et al., 2016; Giesbrecht et al., 2012; Plant et al., 2016). Our corrected results from OSP measurements (58 mmol O_2 m^{-2} d^{-1} in spring) are at the upper range of estimates of these studies and are similar to the anomalously high NCP (~65 mmol O_2 m^{-2} d^{-1}) observed following a large atmospheric dust deposition event in 2008 (see below; Hamme et al., 2010). Only one previous study (Lockwood et al., 2012) reported summertime rates (~84 mmol O_2 m^{-2} d^{-1}) higher than ours. Likewise, along the rest of the off-shelf Line P transect, many of our springtime NCP estimates (>40 mmol O_2 m^{-2} d^{-1}) exceed or represent the upper range of any previously measured values (~10–48 mmol O_2 m^{-2} d^{-1}; Giesbrecht et al., 2012; Hamme et al., 2010; Palevsky et al., 2016).

While interannual variability in NCP partially explains differences between our observations and those of previous studies, it is clear that the contribution of mixing fluxes is also significant. The difference between our results and previous studies is particularly evident in the coastal waters over the continental shelf. At station P4, our average corrected NCP value in August (180 mmol O_2 m^{-2} d^{-1}) is more than fourfold higher than the previous summertime estimates of Hamme et al. (2010) and Giesbrecht et al. (2012). Notably, our uncorrected NCP estimate for this station agrees well with these prior measurements, suggesting that the discrepancy results from an underestimation of NCP in previous studies that have neglected the influence of vertical mixing. This result emphasizes the importance of accounting for negative O_2 fluxes due to subsurface-to-surface mixing, especially in coastal regimes. Net community production estimates derived from previous studies without a correction for mixing should thus be considered as a lower bound on true values, particularly near to the coast.

To our knowledge, only Bushinsky and Emerson (2015), Palevsky et al. (2016), Plant et al. (2016), and Yang et al. (2017) have included physical vertical transport terms when evaluating NCP from O_2 measurements in the Subarctic Pacific. Only Palevsky et al. evaluated spatial patterns in NCP from ship-based data, using model-derived corrections for mixing. Giesbrecht et al. (2012) considered mixing, but found vertical fluxes to be negligible in the spring and summer and therefore excluded any explicit corrections. This result supports our choice to not apply corrections in off-shelf waters where the observed N_2O gradients result in biased mixing coefficients (see section 4.1.5.2).

Beyond the consideration of absolute values, our NCP estimates show spatial and temporal patterns that are consistent with expectations for the Subarctic NE Pacific. Specifically, our data broadly reflect trends in phytoplankton biomass (using chl *a* as a proxy) and demonstrate variability that suggests environmental control from surface nutrient concentrations, seawater temperature, and light availability. The strong NCP gradient from high on-shelf, to relatively low off-shelf production in spring and summer, is an example of this. In

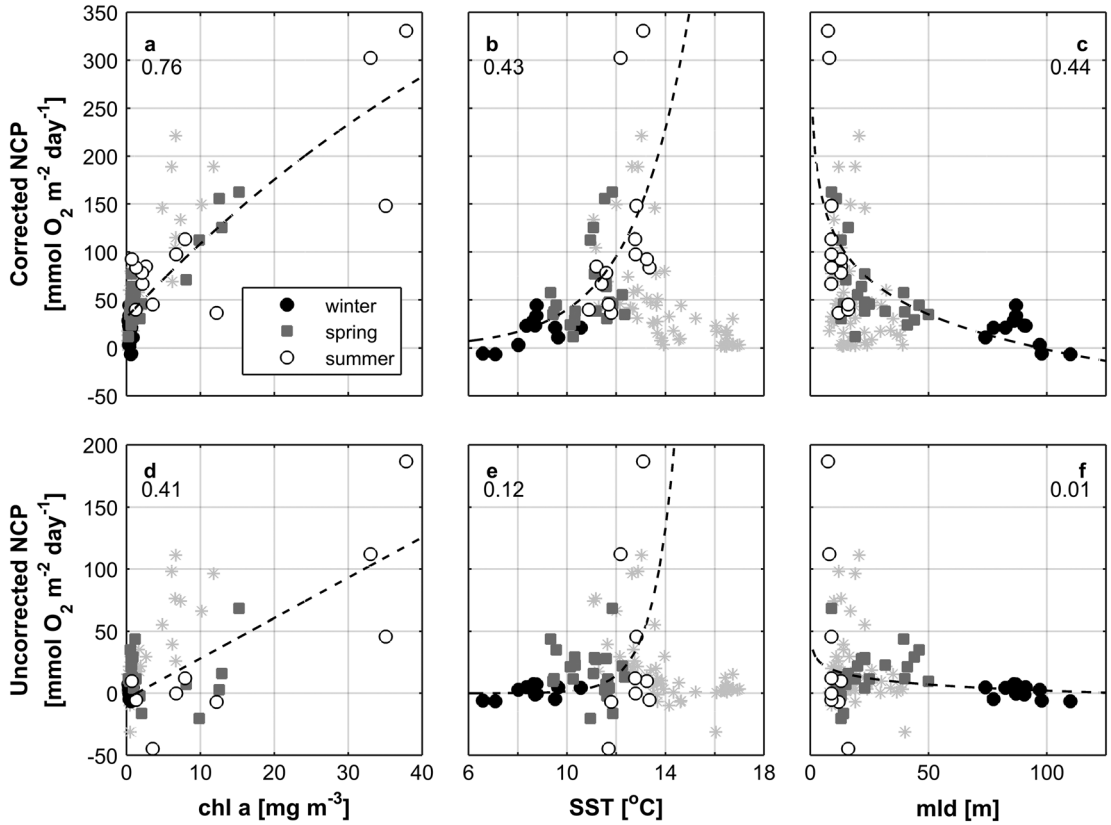

Figure 7. Relationship between corrected NCP and chl *a* (a), SST (b), and mld (c). (d–f) The same relationships for uncorrected NCP. The numbers in each panel represent the correlation coefficients (R^2) for the respective empirical fits. The gray asterisks represent data from regions of presumed N or Fe limitation; these data were excluded from the correlations.

the off-shelf waters of the Line P transect, our measurements likely reflect a progression from wintertime light limitation, to a N- and Fe-limited regime in the late summer, based on insights derived from previous studies (Boyd et al., 1996; Maldonado et al., 1999; Peña & Varela, 2007). The on-shelf waters show typical spring and summer blooms that exceed wintertime production, but these trends are not observed in the uncorrected NCP data, due to the effects of summer upwelling and deep tidal mixing (e.g., in the JF region) that partially mask in situ O_2 production. In some cases, these mixing processes result in apparent net heterotrophy over parts of the continental shelf.

Across broad spatial and temporal scales, our corrected NCP shows strong correlations with chl *a*, SST, and mld (proxy for mixed layer light levels and stratification) (Figures 7a–7c), except under conditions of presumed macronutrient or micronutrient limitation. We infer N limitation in the spring and summer from near-depleted macronutrient concentrations (~50–400 km off-shelf in June and ~50–700 km in August; Figures 2d and 2e), and summertime Fe limitation west of these regions where the significant increase in $NO_3^- + NO_2^-$ concentrations is indicative of previously observed high-nutrient, low-chlorophyll (HNLC) conditions (Harrison et al., 1999; Maldonado et al., 1999). Significantly, we found that the correlations between NCP and the ancillary data were weaker when we used the uncorrected data (based on the R^2 values of empirical best fit equations; Figure 7). This suggests that the corrected values provide a better estimate of the broad spatial patterns and environmental controls on NCP across our survey region. The relationships we observed between NCP and chl, SST, and mld are consistent with results from previous studies in other oceanic systems (Eppley, 1972; Li & Cassar, 2016; Tortell et al., 2015).

Our results also show some localized NCP patterns, such as the wintertime net heterotrophy at OSP (P26), and increased NCP during the spring and summer in the off-shelf waters. While the mechanism driving heterotrophy in subarctic gyres is currently debated, this phenomenon has been observed at OSP previously (Bushinsky & Emerson, 2015; Fassbender et al., 2016; Plant et al., 2016). It should be noted, however, that

we could not apply a mixing correction at station P26 during the winter, and therefore, our NCP represents a lower bound. In contrast, OSP appeared to experience unusually high phytoplankton biomass and NCP in the spring of 2016, coincident with an anomalous increase in chl *a* (Figure 2a). Intermittent Fe fertilization events have been proposed as a mechanism for elevating phytoplankton production at OSP (Boyd et al., 1996). For example, enhanced aerosol deposition (associated with the eruption of Aleutian volcanoes) during summer 2008 was implicated as a source of Fe to the Subarctic Pacific that stimulated enhanced phytoplankton productivity (Hamme et al., 2010). To examine the potential impact of aerosol deposition events at OSP, we evaluated the time series of aerosol optical thickness data, derived from MODIS Aqua satellite products, prior to our occupation in June 2016 (data provided by the NASA Goddard Earth Sciences Data and Information Services Center Giovanni database and retrieved from https://giovanni.gsfc.nasa.gov/giovanni/; Acker & Leptoukh, 2007). This analysis suggested increased aerosol concentrations near OSP during the preceding month (Figure S6h), providing a potential explanation for the elevated chl *a* and NCP. Other regions of high off-shelf productivity (e.g., ~200–500 km off-shelf in February and ~250–600 km in June; Figures 5 and 6) may be attributed to periodic nutrient inputs via coastal eddies (Johnson et al., 2005), periods of mixed layer deepening and entrainment of high subsurface nutrient concentrations, elevated SST, or enhanced stratification. In support of this, satellite-based altimetry showed sea surface height anomalies (data provided by the NASA Physical Oceanography Distributed Active Archive Center and retrieved from https://doi.org/10.5067/SLREFCDRV1; Zlotnicki et al., 2016) indicative of anticyclonic eddies near the Line P transect in June and August (Figures S6e and S6f).

5. Conclusions

Current estimates of ship-based NCP, particularly in coastal waters, will often be biased if investigators neglect vertical mixing fluxes when evaluating surface O_2 budgets. We present refined NCP estimates from five coastal and oceanic cruises in the Subarctic Northeast Pacific, derived using the first field application of a N_2O-based approach to correct for vertical mixing. Our NCP values exceed most past measurements in the study region (due to a combination of natural variability and our consideration of a mixing correction) and show strong correlations with chl *a* concentrations, SST, and mld, providing insight into the environmental controls on biological productivity. We also provide a comprehensive assessment of the N_2O approach in field settings, making recommendations for future applications in our study area and other oceanographic regions. We find that potential surface N_2O production (from nitrification) likely introduces only a small overbias in NCP derived by this approach, although simultaneous measurements of surface N_2O production rates and nitrification yields are required to fully assess the impact of this process. We also discuss scenarios where the N_2O approach should be applied cautiously, or omitted altogether. In particular, N_2O-based corrections are problematic in locations with subsurface minima in $[N_2O]^B$ and corresponding $[O_2]^B$ maxima. Quantifying the magnitude of vertical fluxes from ship-based observations remains a challenge in these regions, since independent and site-specific estimates of vertical mixing rates are necessary. Nonetheless, we conclude that the N_2O correction approach is robust across a range of oceanographic settings, especially in coastal regions where mixing fluxes constitute a substantial part of mixed layer O_2 budgets and where studies of NCP are generally sparse. These coastal waters contribute disproportionately to ocean biogeochemical cycles and are often characterized by significant fine-scale variability, highlighting the utility of underway ship-board $\Delta O_2/Ar$ measurements to estimate surface water NCP.

In light of recent anomalous conditions in the Subarctic Pacific such as large volcanic eruptions (Hamme et al., 2010), the warm-water anomaly (the "blob"; Bond et al., 2015), and observed longer-term trends in sea surface warming, freshening, and deoxygenation (Crawford & Peña, 2013; Whitney & Freeland, 1999), it is important to quantify marine productivity on ecologically relevant spatial and temporal scales. The method employed here has the potential to provide unrivaled surface coverage of NCP estimates corrected for physical mixing. Developing technologies for underway, high-resolution measurements of surface N_2O concentrations and reducing the uncertainties around key assumptions of the method would constitute significant progress in applying this technique. Subsequently, the accumulation of a large NCP database would help to produce regionally tuned satellite algorithms providing basin-scale coverage and enabling better assessment of the future evolution of the ocean's capacity for biomass production and carbon sequestration.

Acknowledgments

We would like to thank all of the individuals involved in each of our 2016 cruises, including chief scientists M. Robert and D. Yelland, participating scientists from the Institute of Ocean Sciences, the University of Victoria, the University of British Columbia, and the University of Washington, and the Captains and crews of the *CCGS J. P. Tully*. We also thank W. Burt for his comments and input on the manuscript and L. Fenwick for her assistance running N_2O samples. Funding for this research was provided by the Natural Sciences and Engineering Research Council of Canada (NSERC). All data presented in this manuscript are available on Pangaea.de (doi:10.1594/PANGAEA.885867). We declare that there are no conflicts of interest associated with the production of this work.

References

Acker, J. G., & Leptoukh, G. (2007). Online analysis enhances use of NASA Earth science data. *Eos, Transactions American Geophysical Union*, *88*(2), 14–17.

Allen, S. E., & Durrieu de Madron, X. (2009). A review of the role of submarine canyons in deep-ocean exchange with the shelf. *Ocean Science*, *5*(4), 607–620. https://doi.org/10.5194/os-5-607-2009

Arévalo-Martínez, D. L., Beyer, M., Krumbholz, M., Piller, I., Kock, A., Steinhoff, T., et al. (2013). A new method for continuous measurements of oceanic and atmospheric N_2O, CO and CO_2: Performance of off-axis integrated cavity output spectroscopy (OA-ICOS) coupled to non-dispersive infrared detection (NDIR). *Ocean Science*, *9*(6), 1071–1087. https://doi.org/10.5194/os-9-1071-2013

Atlas, R., Hoffman, R. N., Ardizzone, J., Leidner, S. M., Jusem, J. C., Smith, D. K., & Gombos, D. (2011). A cross-calibrated, multiplatform ocean surface wind velocity product for meteorological and oceanographic applications. *Bulletin of the American Meteorological Society*, *92*(2), 157–174. https://doi.org/10.1175/2010BAMS2946.1

Bakun, A. (1973). Coastal upwelling indices, west coast of North America, 1946-71. U.S. Dept. of Commerce, NOAA Tech. Rep., NMFS SSRF-671, 1–103.

Bange, H., Rapsomanikis, S., & Andreae, M. (1996). Nitrous oxide in coastal waters. *Global Biogeochemical Cycles*, *10*(1), 197–207. https://doi.org/10.1029/95GB03834

Barwell-Clarke, J., & Whitney, F. (1996). Institute of Ocean Sciences nutrient methods and analysis. *Canadian Technical Report of Hydrography and Ocean Sciences*, *182*, 1–42.

Bond, N. A., Cronin, M. F., Freeland, H., & Mantua, N. (2015). Causes and impacts of the 2014 warm anomaly in the NE Pacific. *Geophysical Research Letters*, *42*, 3414–3420. https://doi.org/10.1002/2015GL063306

Bonjean, F., & Lagerloef, G. S. E. (2002). Diagnostic model and analysis of the surface currents in the tropical Pacific Ocean. *Journal of Physical Oceanography*, *32*(10), 2938–2954. https://doi.org/10.1175/1520-0485(2002)032%3C2938:DMAAOT%3E2.0.CO;2

Boyd, P. W., Muggli, D. L., Varela, D. E., Goldblatt, R. H., Chretien, R., Orians, K. J., & Harrison, P. J. (1996). In vitro iron enrichment experiments in NE subarctic Pacific. *Marine Ecology Progress Series*, *136*, 179–193. https://doi.org/10.3354/meps136179

Brown, Z. W., Casciotti, K. L., Pickart, R. S., Swift, J. H., & Arrigo, K. R. (2015). Aspects of the marine nitrogen cycle of the Chukchi Sea shelf and Canada Basin. *Deep-Sea Research Part II: Topical Studies in Oceanography*, *118*, 73–87. https://doi.org/10.1016/j.dsr2.2015.02.009

Bushinsky, S. M., & Emerson, S. (2015). Marine biological production from in situ oxygen measurements on a profiling float in the subarctic Pacific Ocean. *Global Biogeochemical Cycles*, *29*, 2050–2060. https://doi.org/10.1002/2015GB005251

Bylhouwer, B., Ianson, D., & Kohfeld, K. (2013). Changes in the onset and intensity of wind-driven upwelling and downwelling along the North American Pacific coast. *Journal of Geophysical Research: Oceans*, *118*, 2565–2580. https://doi.org/10.1002/jgrc.20194

Capelle, D. W., Dacey, J. W., & Tortell, P. D. (2015). An automated, high through-put method for accurate and precise measurements of dissolved nitrous-oxide and methane concentrations in natural waters. *Limnology and Oceanography: Methods*, *13*(7), 345–355. https://doi.org/10.1002/lom3.10029

Capelle, D. W., & Tortell, P. D. (2016). Factors controlling methane and nitrous-oxide variability in the southern British Columbia coastal upwelling system. *Marine Chemistry*, *179*(2016), 56–67. https://doi.org/10.1016/j.marchem.2016.01.011

Carpenter, J. H. (1965). The Chesapeake Bay institute technique for the Winkler dissolved oxygen method. *Limnology and Oceanography*, *10*(1), 141–143. https://doi.org/10.4319/lo.1965.10.1.0141

Cassar, N., Barnett, B. A., Bender, M. L., Kaiser, J., Hamme, R. C., & Tilbrook, B. (2009). Continuous high-frequency dissolved O_2/Ar measurements by equilibrator inlet mass spectrometry. *Analytical Chemistry*, *81*(5), 1855–1864. https://doi.org/10.1021/ac802300u

Cassar, N., Nevison, C. D., & Manizza, M. (2014). Correcting oceanic O_2/Ar-net community production estimates for vertical mixing using N_2O observations. *Geophysical Research Letters*, *41*, 8961–8970. https://doi.org/10.1002/2014GL062040

Castro-Morales, K., Cassar, N., Shoosmith, D. R., & Kaiser, J. (2013). Biological production in the Bellingshausen Sea from oxygen-to-argon ratios and oxygen triple isotopes. *Biogeosciences*, *10*(4), 2273–2291. https://doi.org/10.5194/bg-10-2273-2013

Codispoti, L. A., Yoshinari, T., & Devol, A. H. (2005). Suboxic respiration in the oceanic water column. In *Respiration in aquatic ecosystems* (pp. 225–247). Oxford, UK: Oxford University Press. https://doi.org/10.1093/acprof:oso/9780198527084.003.0012

Cohen, Y., & Gordon, L. I. (1979). Nitrous oxide production in the ocean. *Journal of Geophysical Research*, *84*(C1), 347–353. https://doi.org/10.1029/JC084iC01p00347

Craig, H., & Hayward, T. (1987). Oxygen supersaturation in the ocean: Biological versus physical contributions. *Science*, *235*(4785), 199–202. https://doi.org/10.1126/science.235.4785.199

Crawford, W. R., & Peña, M. A. (2013). Declining oxygen on the British Columbia continental shelf. *Atmosphere-Ocean*, *51*(1), 88–103. https://doi.org/10.1080/07055900.2012.753028

Crawford, W. R., & Thomson, R. E. (1991). Physical oceanography of the western Canadian continental shelf. *Continental Shelf Research*, *11*(8-10), 669–683. https://doi.org/10.1016/0278-4343(91)90073-F

Cronin, M. F., Pellan, N. A., Emerson, S. R., & Crawford, W. R. (2015). Estimating diffusivity from the mixed layer heat and salt balances in the North Pacific. *Journal of Geophysical Research: Oceans*, *120*, 7346–7362. https://doi.org/10.1002/2015JC011010

Dore, J. E., & Karl, D. M. (1996). Nitrification in the euphotic zone as a source for nitrite, nitrate, and nitrous oxide at station ALOHA. *Limnology and Oceanography*, *41*(8), 1619–1628. https://doi.org/10.4319/lo.1996.41.8.1619

Emerson, S., Ito, T., & Hamme, R. C. (2012). Argon supersaturation indicates low decadal-scale vertical mixing in the ocean thermocline. *Geophysical Research Letters*, *39*, L18610. https://doi.org/10.1029/2012GL053054

Emerson, S., Quay, P., Karl, D., Winn, C., Tupas, L., & Landry, M. (1997). Experimental determination of the organic carbon flux from open-ocean surface waters. *Nature*, *389*(6654), 951–954. https://doi.org/10.1038/40111

Eppley, R. W. (1972). Temperature and phytoplankton growth in the sea. *Fishery Bulletin*, *70*, 1063–1085.

Earth Space Research (2009). OSCAR third degree resolution ocean surface currents. Ver. 1. PO.DAAC, CA, USA. https://doi.org/10.5067/OSCAR-03D01

Farías, L., Castro-González, M., Cornejo, M., Charpentier, J., Faúndez, J., Boontanon, N., & Yoshida, N. (2009). Denitrification and nitrous oxide cycling within the upper oxycline of the eastern tropical South Pacific oxygen minimum zone. *Limnology and Oceanography*, *54*(1), 132–144. https://doi.org/10.4319/lo.2009.54.1.0132

Fassbender, A. J., Sabine, C. L., & Cronin, M. F. (2016). Net community production and calcification from 7 years of NOAA Station Papa Morring measurements. *Global Biogeochemical Cycles*, *30*, 250–267. https://doi.org/10.1002/2015GB005205

Fenwick, L., Capelle, D., Damm, E., Zimmermann, S., Williams, W. J., Vagle, S., & Tortell, P. D. (2017). Methane and nitrous oxide distributions across the North American Arctic Ocean during summer, 2015. *Journal of Geophysical Research: Oceans*, *122*, 390–412. https://doi.org/10.1002/2016JC012493

Frame, C. H., & Casciotti, K. L. (2010). Biogeochemical controls and isotopic signatures of nitrous oxide production by a marine ammonia-oxidizing bacterium. *Biogeosciences Discussions*, *7*(9), 2695–2709. https://doi.org/10.5194/bg-7-2695-2010

Garcia, H. E., & Gordon, L. I. (1992). Oxygen solubility in seawater: Better fitting equations. *Limnology and Oceanography*, *37*(6), 1307–1312. https://doi.org/10.2307/2837876

Garcia, H. E., & Gordon, L. I. (1993). Erratum: Oxygen solubility in seawater: Better fitting equations. *Limnology and Oceanography*, *38*, 656.

Giesbrecht, K. E., Hamme, R. C., & Emerson, S. R. (2012). Biological productivity along Line P in the subarctic northeast Pacific: In situ versus incubation-based methods. *Global Biogeochemical Cycles*, *26*, GB3028. https://doi.org/10.1029/2012GB004349

Goreau, T. J., Kaplan, W. A., Wofsy, S. C., McElroy, M. B., Valois, F. W., & Watson, S. W. (1980). Production of NO_2^- and N_2O by nitrifying bacteria at reduced concentrations of oxygen. *Applied and Environmental Microbiology*, *40*(3), 526–532.

Grefe, I., & Kaiser, J. (2014). Equilibrator-based measurements of dissolved nitrous oxide in the surface ocean using an integrated cavity output laser absorption spectrometer. *Ocean Science*, *10*(3), 501–512. https://doi.org/10.5194/os-10-501-2014

Grundle, D. S., Juniper, S. K., & Giesbrecht, K. E. (2013). Euphotic zone nitrification in the NE subarctic Pacific: Implications for measurements of new production. *Marine Chemistry*, *155*(2013), 113–123. https://doi.org/10.1016/j.marchem.2013.06.004

Grundle, D. S., Maranger, R., & Juniper, S. K. (2012). Upper water column nitrous oxide distributions in the northeast subarctic Pacific Ocean. *Atmosphere-Ocean*, *50*(4), 475–486. https://doi.org/10.1080/07055900.2012.727779

Hall, B. D., Dutton, G. S., & Elkins, J. W. (2007). The NOAA nitrous oxide standard scale for atmospheric observations. *Journal of Geophysical Research*, *112*, D09305. https://doi.org/10.1029/2006JD007954

Hamme, R. C., Cassar, N., Lance, V. P., Vaillancourt, R. D., Bender, M. L., Strutton, P. G., et al. (2012). Dissolved O_2/Ar and other methods reveal rapid changes in productivity during a Lagrangian experiment in the Southern Ocean. *Journal of Geophysical Research*, *117*, C00F12. https://doi.org/10.1029/2011JC007046

Hamme, R. C., & Emerson, S. R. (2002). Mechanisms controlling the global oceanic distribution of the inert gases argon, nitrogen and neon. *Geophysical Research Letters*, *29*(23), 2120. https://doi.org/10.1029/2002GL015273

Hamme, R. C., & Emerson, S. R. (2006). Constraining bubble dynamics and mixing with dissolved gases: Implications for productivity measurements by oxygen mass balance. *Journal of Marine Research*, *64*(1), 73–95. https://doi.org/10.1357/002224006776412322

Hamme, R. C., Webley, P. W., Crawford, W. R., Whitney, F. A., Degrandpre, M. D., Emerson, S. R., et al. (2010). Volcanic ash fuels anomalous plankton bloom in subarctic northeast Pacific. *Geophysical Research Letters*, *37*, L19604. https://doi.org/10.1029/2010GL044629

Harrison, P. J., Boyd, P. W., Varela, D. E., Takeda, S., Shiomoto, A., & Odate, T. (1999). Comparison of factors controlling phytoplankton productivity in the NE and NW subarctic Pacific gyres. *Progress in Oceanography*, *43*(2-4), 205–234. https://doi.org/10.1016/S0079-6611(99)00015-4

Ho, D. T., Law, C. S., Smith, M. J., Schlosser, P., Harvey, M., & Hill, P. (2006). Measurements of air-sea gas exchange at high wind speeds in the Southern Ocean: Implications for global parameterizations. *Geophysical Research Letters*, *33*, L16611. https://doi.org/10.1029/2006GL026817

Horrigan, S. G., Carlucci, A. F., & Williams, P. M. (1981). Light inhibition of nitrification in sea-surface films. *Journal of Marine Research*, *39*(3), 557–565.

Howard, E., Emerson, S., Bushinsky, S., & Stump, C. (2010). The role of net community production in air-sea carbon fluxes at the North Pacific subarctic-subtropical boundary region. *Limnology and Oceanography*, *55*(6), 2585–2596. https://doi.org/10.4319/lo.2010.55.6.2585

Ianson, D., & Allen, S. E. (2002). A two-dimensional nitrogen and carbon flux model in a coastal upwelling region. *Global Biogeochemical Cycles*, *16*(1), 1011. https://doi.org/10.1029/2001GB001451

Jin, X., Najjar, R. G., Louanchi, F., & Doney, S. C. (2007). A modeling study of the seasonal oxygen budget of the global ocean. *Journal of Geophysical Research*, *112*, C05017. https://doi.org/10.1029/2006JC003731

Johnson, W. K., Miller, L. A., Sutherland, N. E., & Wong, C. S. (2005). Iron transport by mesoscale Haida eddies in the Gulf of Alaska. *Deep-Sea Research Part II: Topical Studies in Oceanography*, *52*(7-8), 933–953. https://doi.org/10.1016/j.dsr2.2004.08.017

Jonsson, B. F., Doney, S. C., Dunne, J., & Bender, M. (2013). Evaluation of the Southern Ocean O_2/Ar-based NCP estimates in a model framework. *Journal of Geophysical Research: Biogeosciences*, *118*, 385–399. https://doi.org/10.1002/jgrg.20032

Kaiser, J., Reuer, M. K., Barnett, B., & Bender, M. L. (2005). Marine productivity estimates from continuous O_2/Ar ratio measurements by membrane inlet mass spectrometry. *Geophysical Research Letters*, *32*, L19605. https://doi.org/10.1029/2005GL023459

Kalnay, E., Kanamitsu, M., Kistler, R., Collins, W., Deaven, D., Gandin, L., et al. (1996). The NCEP/NCAR 40-year reanalysis project. *Bulletin of the American Meteorological Society*, *77*(3), 437–471. https://doi.org/10.1175/1520-0477(1996)077%3C0437:TNYRP%3E2.0.CO;2

Keeling, R. F., & Shertz, S. R. (1992). Seasonal and interannual variations in atmospheric oxygen and implications for the global carbon cycle. *Nature*, *358*(6389), 723–727. https://doi.org/10.1038/358723a0

Kundu, P. K., Cohen, I. M., & Dowling, D. R. (2012). *Fluid mechanics* (5th ed.). Amsterdam, Netherlands: Elsevier.

Laws, E. A. (1991). Photosynthetic quotients, new production and net community production in the open ocean. *Deep Sea Research*, *38*(1), 143–167. https://doi.org/10.1016/0198-0149(91)90059-O

Li, Z., & Cassar, N. (2016). Satellite estimates of net community production based on O_2/Ar observations and comparison to other estimates. *Global Biogeochemical Cycles*, *30*, 735–752. https://doi.org/10.1002/2015GB005314

Lockwood, D., Quay, P. D., Kavanaugh, M. T., Juranek, L. W., & Feely, R. A. (2012). High-resolution estimates of net community production and air-sea CO_2 flux in the northeast Pacific. *Global Biogeochemical Cycles*, *26*, GB4010. https://doi.org/10.1029/2012GB004380

Luz, B., & Barkan, E. (2009). Net and gross oxygen production from O_2/Ar, $^{17}O/^{16}O$ and $^{18}O/^{16}O$ ratios. *Aquatic Microbial Ecology*, *56*, 133–145. https://doi.org/10.3354/ame01296

Maldonado, M. T., Boyd, P. W., Harrison, P. J., & Price, N. M. (1999). Co-limitation of phytoplankton growth by light and Fe during winter in the NE subarctic Pacific Ocean. *Deep-Sea Research Part II: Topical Studies in Oceanography*, *46*(11-12), 2475–2485. https://doi.org/10.1016/S0967-0645(99)00072-7

Manning, C. C., Stanley, R. H. R., Nicholson, D. P., Smith, J. M., Pennington, J. T., Fewings, M. R., et al. (2017). Impact of recently upwelled water on productivity investigated using in situ and incubation-based methods in Monterey Bay. *Journal of Geophysical Research: Oceans*, *122*, 1901–1926. https://doi.org/10.1002/2016JC012306

NASA Goddard Space Flight Center, Ocean Ecology Laboratory, Ocean Biology Processing Group (2014a). Moderate-Resolution Imaging Spectroradiometer (MODIS) Aqua daytime 11 μ SST data. NASA, OB.DAAC. https://doi.org/10.5067/MODSA-1D9D4

NASA Goddard Space Flight Center, Ocean Ecology Laboratory, Ocean Biology Processing Group (2014b). Moderate-Resolution Imaging Spectroradiometer (MODIS) Aqua nighttime 11 μ SST data. NSAS OB.DAAC. https://doi.org/10.5067/MODSA-1D9N4

Nevison, C., Butler, J. H., & Elkins, J. W. (2003). Global distribution of N_2O and the ΔN_2O-AOU yield in the subsurface ocean. *Global Biogeochemical Cycles*, *17*(4), 1119. https://doi.org/10.1029/2003GB002068

Oudot, C., Andrie, C., & Montel, Y. (1990). Nitrous oxide production in the tropical Atlantic Ocean. *Deep Sea Research*, *37*(2), 183–202. https://doi.org/10.1016/0198-0149(90)90123-D

Palevsky, H. I., Quay, P. D., Lockwood, D. E., & Nicholson, D. P. (2016). The annual cycle of gross primary production, net community production, and export efficiency across the North Pacific Ocean. *Global Biogeochemical Cycles*, *30*, 361–380. https://doi.org/10.1002/2015GB005318

Peña, M. A., & Varela, D. E. (2007). Seasonal and interannual variability in phytoplankton and nutrient dynamics along Line P in the NE subarctic Pacific. *Progress in Oceanography*, *75*(2), 200–222. https://doi.org/10.1016/j.pocean.2007.08.009

Plant, J. N., Johnson, K. S., Sakamoto, C. M., Jannasch, H. W., Coletti, L. J., Riser, S. C., & Swift, D. D. (2016). Net community production at Ocean Station Papa observed with nitrate and oxygen sensors on profiling floats. *Global Biogeochemical Cycles*, *30*, 859–879. https://doi.org/10.1002/2015GB005349.Received

Rees, A. P., Owens, N. J. P., & Upstill-Goddard, R. C. (1997). Nitrous oxide in the Bellingshausen Sea and Drake Passage. *Journal of Geophysical Research*, *102*(C2), 3383–3391. https://doi.org/10.1029/96JC03350

Reuer, M. K., Barnett, B. A., Bender, M. L., Falkowski, P. G., & Hendricks, M. B. (2007). New estimates of Southern Ocean biological production rates from O_2/Ar ratios and the triple isotope composition of O_2. *Deep-Sea Research Part I: Oceanographic Research Papers*, *54*(6), 951–974. https://doi.org/10.1016/j.dsr.2007.02.007

Rousseau, S., Kunze, E., Dewey, R., Bartlett, K., & Dower, J. (2010). On turbulence production by swimming marine organisms in the open ocean and coastal waters. *Journal of Physical Oceanography*, *40*(9), 2107–2121. https://doi.org/10.1175/2010JPO4415.1

Santoro, A. E., Buchwald, C., McIlvin, M. R., & Casciotti, K. L. (2011). Isotopic signature of N_2O produced by marine ammonia-oxidizing archaea. *Science*, *333*(6047), 1282–1285. https://doi.org/10.1126/science.1208239

Santoro, A. E., Casciotti, K. L., & Francis, C. A. (2010). Activity, abundance and diversity of nitrifying archaea and bacteria in the central California Current. *Environmental Microbiology*, *12*(7), 1989–2006. https://doi.org/10.1111/j.1462-2920.2010.02205.x

Shulenberger, E., & Reid, J. L. (1981). The Pacific shallow oxygen maximum, deep chlorophyll maximum, and primary productivity, reconsidered. *Deep Sea Research*, *28*(9), 901–919. https://doi.org/10.1016/0198-0149(81)90009-1

Smith, J. M., Casciotti, K. L., Chavez, F. P., & Francis, C. A. (2014). Differential contributions of archaeal ammonia oxidizer ecotypes to nitrification in coastal surface waters. *The ISME Journal*, *8*(8), 1704–1714. https://doi.org/10.1038/ismej.2014.11

Stanley, R. H. R., Kirkpatrick, J. B., Cassar, N., Barnett, B. A., & Bender, M. L. (2010). Net community production and gross primary production rates in the western equatorial Pacific. *Global Biogeochemical Cycles*, *24*, GB4001. https://doi.org/10.1029/2009GB003651

Tabata, S. (1975). The general circulation of the Pacific Ocean and a brief account of the oceanographic structure of the North Pacific Ocean. *Atmosphere*, *13*, 1034–1054. https://doi.org/10.1080/00046973.1976.9648398

Teeter, L. (2014). Modelling oxygen and argon to improve estimation of net community productivity in a coastal upwelling zone using ΔO_2/Ar. (MSc. Thesis). University of Victoria, Victoria, BC, Canada. Retrieved from https://dspace.library.uvic.ca//handle/1828/5819

Tortell, P. D. (2005). Dissolved gas measurements in oceanic waters made by membrane inlet mass spectrometry. *Limnology and Oceanography: Methods*, *3*(1), 24–37. https://doi.org/10.4319/lom.2005.3.24

Tortell, P. D., Bittig, H. C., Körtzinger, A., Jones, E. M., & Hoppema, M. (2015). Biological and physical controls on N_2, O_2, and CO_2 distributions in contrasting Southern Ocean surface waters. *Global Biogeochemical Cycles*, *29*, 994–1013. https://doi.org/10.1002/2014GB004975

Tortell, P. D., Guéguen, C., Long, M. C., Payne, C. D., Lee, P., & DiTullio, G. R. (2011). Spatial variability and temporal dynamics of surface water pCO_2, ΔO_2/Ar and dimethylsulfide in the Ross Sea, Antarctica. *Deep-Sea Research Part I: Oceanographic Research Papers*, *58*(3), 241–259. https://doi.org/10.1016/j.dsr.2010.12.006

Tortell, P. D., Merzouk, A., Ianson, D., Pawlowicz, R., & Yelland, D. R. (2012). Influence of regional climate forcing on surface water pCO_2, O_2/Ar and dimethylsulfide (DMS) along the southern British Columbia coast. *Continental Shelf Research*, *47*(2012), 119–132. https://doi.org/10.1016/j.csr.2012.07.007

Ulfsbo, A., Cassar, N., Korhonen, M., van Heuven, S., Hoppema, M., Kattner, G., & Anderson, L. G. (2014). Late summer net community production in the central Arctic Ocean using multiple approaches. *Global Biogeochemical Cycles*, *28*, 1129–1148. https://doi.org/10.1002/2014GB004833

Varela, D. E., & Harrison, P. J. (1999). Seasonal variability in nitrogenous nutrition of phytoplankton assemblages in the northeastern subarctic Pacific Ocean. *Deep-Sea Research Part II: Topical Studies in Oceanography*, *46*(11-12), 2505–2538. https://doi.org/10.1016/S0967-0645(99)00074-0

Volk, T., & Hoffert, M. I. (1985). Ocean carbon pumps: Analysis of relative strengths and efficiencies in ocean-driven atmospheric CO_2 changes. In E. T. Sundquist & W. S. Broecker (Eds.), *The carbon cycle and atmospheric CO_2: Natural variations Archean to present* (pp. 99–110). Washington, DC: American Geophysical Union. https://doi.org/10.1029/GM032p0099

Wanninkhof, R. (2014). Relationship between wind speed and gas exchange over the ocean revisited. *Limnology and Oceanography: Methods*, *97*(C5), 7373–7362. https://doi.org/10.1029/92JC00188

Ward, B. B. (2000). Nitrification and the marine nitrogen cycle. In D. Kirchman (Ed.), *Microbial ecology* (pp. 427–454). New York: Wiley-Liss.

Ward, B. B. (2005). Temporal variability in nitrification rates and related biogeochemical factors in Monterey Bay, California, USA. *Marine Ecology Progress Series*, *292*, 97–109. https://doi.org/10.3354/meps292097

Ware, D. M., & Thomson, R. E. (2005). Bottom-up ecosystem trophic dynamics determine fish production in the northeast Pacific. *Science*, *308*(5726), 1280–1284. https://doi.org/10.1126/science.1109049

Weeding, B., & Trull, T. W. (2014). Hourly oxygen and total gas tension measurements at the Southern Ocean time series site reveal winter ventilation and spring net community production. *Journal of Geophysical Research: Oceans*, *119*, 348–358. https://doi.org/10.1002/2013JC009302

Weiss, R. F., & Price, B. A. (1980). Nitrous oxide solubility in water and seawater. *Marine Chemistry*, *8*(4), 347–359. https://doi.org/10.1016/0304-4203(80)90024-9

Welschmeyer, N. A. (1994). Fluorometric analysis of chlorophyll a in the presence of chlorophyll b and pheopigments. *Limnology and Oceanography*, *39*(8), 1985–1992. https://doi.org/10.4319/lo.1994.39.8.1985

Whalen, C. B., Talley, L. D., & MacKinnon, J. A. (2012). Spatial and temporal variability of global ocean mixing inferred from Argo profiles. *Geophysical Research Letters*, *39*, L18612. https://doi.org/10.1029/2012GL053196

Whitney, F. A., Crawford, W. R., & Harrison, P. J. (2005). Physical processes that enhance nutrient transport and primary productivity in the coastal and open ocean of the subarctic NE Pacific. *Deep-Sea Research Part II: Topical Studies in Oceanography*, *52*(5-6), 681–706. https://doi.org/10.1016/j.dsr2.2004.12.023

Whitney, F. A., & Freeland, H. J. (1999). Variability in upper-ocean water properties in the NE Pacific Ocean. *Deep-Sea Research Part II: Topical Studies in Oceanography*, *46*(11-12), 2351–2370. https://doi.org/10.1016/S0967-0645(99)00067-3

Whitney, F. A., Wong, C. S., & Boyd, P. W. (1998). Interannual variability in nitrate supply to surface waters of the northeast Pacific Ocean. *Marine Ecology Progress Series*, *170*, 15–23. https://doi.org/10.3354/meps170015

Yang, B., Emerson, S. R., & Bushinsky, S. M. (2017). Annual net community production in the subtropical Pacific Ocean from in-situ oxygen measurements on profiling floats. *Global Biogeochemical Cycles*, *31*, 728–744. https://doi.org/10.1002/2016GB005545

Yoshida, N., Morimoto, H., Hirano, M., Koike, I., Matsuo, S., Wada, E., et al. (1989). Nitrification rates and ^{15}N abundances of N_2O and NO_3^- in the western North Pacific. *Nature*, *342*(6252), 895–897. https://doi.org/10.1038/342895a0

Yoshinari, T. (1976). Nitrous oxide in the sea. *Marine Chemistry*, *4*(2), 189–202. https://doi.org/10.1016/0304-4203(76)90007-4

Zamora, L. M., & Oschlies, A. (2014). Surface nitrification: A major uncertainty in marine N_2O emissions. *Geophysical Research Letters*, *41*, 4247–4253. https://doi.org/10.1002/2014GL060556

Zlotnicki, V., Qu, Z., & Willis, J. (2016). JPL MEaSUREs gridded sea surface height anomalies version 1609. Ver. 1609. PO.DAAC, CA, USA. https://doi.org/10.5067/SLREF-CDRV1